DEEP WATER RENEWAL DURING WINTERTIME STRATIFICATION IN A DEEP, FRESHWATER, THERMOBARICALLY STRATIFIED LAKE

by

Lydia Smith

B.S., Salisbury University, 2008

A THESIS SUBMITTED IN PARTIAL FULFILLMENT OF

THE REQUIREMENTS FOR THE DEGREE OF

MASTER OF APPLIED SCIENCE

in

THE FACULTY OF GRADUATE AND POSTDOCTORAL STUDIES

(Civil Engineering)

THE UNIVERSITY OF BRITISH COLUMBIA

(Vancouver)

September 2020

The following individuals certify that they have read, and recommend to the Faculty of Graduate and Postdoctoral Studies for acceptance, a thesis entitled:

Deep Water Renewal During Wintertime Stratification in a Deep, Freshwater, Thermobarically Stratified Lake

submitted by Lydia Smith in partial fulfillment of the requirements for

the degree of Master of Applied Science

in Civil Engineering

Examining Committee:

Dr. Bernard Laval, Head of Department, Department of Civil Engineering, UBC

Supervisor

Dr. Svein Vagle, Research Scientist, Department of Fisheries and Oceans, Institute of Ocean Sciences

Supervisory Committee Member

Abstract

Thermobarically stratified Quesnel Lake shows relatively high rates of hypolimnetic mixing and transport over its winter (inverse) stratification period. A decade-long data set reveals annual winter trends of warming and cooling at 500 m depth, field measurements record increasing hypolimnetic oxygen levels between fall and summer, demonstrating regular ventilation. This research describes processes responsible for the ventilation of the deep hypolimnetic water of Quesnel Lake. Temperature records from moored instruments, and conductivity, temperature, and depth (CTD) profiles were processed to assess transport and mixing in the lake. Local weather stations, regional government data, and modelled data were used to calculate atmospheric forcing at the surface of the lake. These data were compared to find links between atmospheric events and deep-water behavior over the winter of 2006-2007. The results show that the deep water is ventilated by wintertime thermobaric instabilities induced by baroclinic seiche, and by a prolonged spring turnover. Turbulent mixing from seiche homogenizes the bottom water (within 0.02ºC) to a maximum height of ~400 m above the lake bottom. Deepening of the surface mixed layer is aided by the homogenized bottom layer to produce a full spring turnover. This study supports previous research on Quesnel Lake, demonstrating that wind forcing is an effective mixing and transport mechanism even in the deepest region of the lake.

Lay Summary

Lakes are vital systems for ecological health and human societies. The internal motions of water in lakes maintain water quality by transporting nutrients, gases, and heat throughout the lake body. This research centers on understanding deep water mixing processes in Quesnel Lake, British Columbia, Canada. Lake temperature records show all 500 m of Quesnel Lake are partially mixed annually despite being one of the deepest lakes in the world. The majority of deep water renewal takes place over winter when storms create basin-wide standing waves known as ‘seiche’. This leads to near-surface water sinking into deeper water, replenishing dissolved oxygen levels. These same seiches create mixing in the bottom waters. The well-mixed bottom layer aids surface mixing to create a full spring turnover, an event where all 500 m of the water column become effectively homogenized allowing free circulation of nutrients, gases, and heat through the water column.

Preface

The writing and data analysis of this thesis was completed by the author with guidance from Dr. Bernard Laval.

Field data for this work was collected by various affiliates of the University of British Columbia, University of Northern British Columbia, Quesnel River Research Center, and the Institute of Ocean Sciences. Certain data was obtained through publicly available online data archives provided by Government Canada and the National Renewable Energy Lab as outlined in Chapter 3: Methods.

Figure 4.1.2 was created by Dr Bernard Laval and displayed at the Physical Processes in Natural Waters conference in Trento, Italy, 2014.

Table of Contents

List of Figures

List of Symbols

α	Thermal expansion coefficient
α_S	Alpha shortwave
α_L	Alpha longwave
$A(z)$	Area with depth (z)
B_0	Surface buoyancy flux
°C	Degrees Celsius
c_p	Heat capacity of water
C_d	Drag coefficient
$\frac{dH}{dt}$	Time derivative of heat content
dz	Change in depth
g	Gravity
g'	Augmented gravity
$H_{content}$	Heat content
H_{eff}	Effective depth
h_1	Depth of layer 1
h_2	Depth of layer 2
H_f	Heat flux
Hl	Latent heat
Hs	Sensible heat
H_Q	Heat content
n	Number of layers
ρ	Density of water
k	Van Kármán constant
L	Basin length
L_{MO}	Monin-Obukhov depth
LW	Longwave radiation
ρ_{air}	Density of air
ρ_0	Reference density
Q_{in}	Incoming heat

$\boldsymbol{Q_{out}}$	Outgoing heat
$\boldsymbol{SW}$	Shortwave radiation
$\boldsymbol{T}$	Temperature
$\boldsymbol{\tau}$	Wind stress
$\boldsymbol{u}$	Wind speed
$\boldsymbol{u_*}$	Wind shear
$\boldsymbol{W}$	Wedderburn number
$\boldsymbol{z}$	Depth

List of Abbreviations

BC	British Columbia
CTD	Conductivity, Temperature, and Depth
DFO	Department of Fisheries and Oceans
DO	Dissolved oxygen
GSW	Gibbs Sea Water
IOS	The Institute of Ocean Sciences
MPMC	Mount Polley Mining Company
NREL	National Renewable Energy Laboratory
NSRDB	National Solar Radiation Database
RH	Relative humidity
S	Salinity
STP	Standard temperature and pressure
TMD	Temperature of maximum density
TKE	Turbulent kinetic energy
UBC	University of British Columbia
UNBC	University of Northern British Columbia

Acknowledgements

The list of thanks I have to give is longer than the space allowed. However, I would particularly like to thank the following:

- Dr. Bernard Laval for accepting me as a student, giving prompt, helpful, and insightful feedback, and ultimately leading me to finishing this thesis and gaining my degree. Its been great learning from you as a student, and discussing world events, politics, or other perils along the way.
- Dr. Svein Vagle, brilliant scientist and boat captain extraordinaire! I have enjoyed each and every one of our encounters. Thank you for the wonderful mooring servicing trips at Quesnel and for your feedback on my thesis. May we drink wine and download data again one day!
- The EFM lab group for being so much more than colleagues! Each and every single one of you has made my time a UBC just that much more wonderful. I am so lucky to have been able to work amongst such intelligent, welcoming, dynamic, and fun people.
- Cat Chat (AKA Kelly Graves and Sarah Chang) gets a special shout out for lending support and focus during these strange Covid-19 times. I honestly do not think I could have completed my thesis without our daily check-ins. To cats, friendship, water, and higher education!
- Finally, to my family and my darling Tuff Kitty; I've had such a great life. I have each of you to thank for that.

Chapter 1: Introduction

To the general observer, a lake may appear as a quiescent body of water. However, lakes contain dynamic structures and respond to forcing from the environment. The vertical structure of lakes is created by water of varying densities creating stable or unstable regions. A stable water column will stratify, whereas an unstable water column will mix until stabilization is attained. These cycles of stabilization and mixing in lakes have major impacts on the water quality and surrounding ecology of a lake due to their influence on the distribution of heat and suspended and dissolved materials in the system (Hutter, Wang, & Chubarenko, 2011; Imboden & Wuest, 1995).

Lakes have been researched for centuries, but most of this research has focused on water in shallow- to mid-depth lakes. The deep water of very deep lakes (>200 m as defined in section 2.2) had been somewhat inaccessible using past technologies. Today, advancements in scientific equipment and techniques have greatly improved the accessibility of deep water. Sensors can record deeper, faster, and with far greater accuracy than was historically possible.

Interest in deep lake mixing and stratification has increased as the impacts of climate change become better understood (Vincent, 2009). In temperate climates, very deep lakes can become thermobarically stratified, adding complexity to their cycling process. A lake being thermobarically stratified means the slight compressibility of water, particularly near the temperature of maximum density (section 2.2) must be considered in the stratification and mixing processes (Carmack & Weiss, 1991; Farmer & Carmack, 1981). Research indicates lakes of certain geometries may have deep water that is unaffected by a warming climate, due to lack of regular circulation; for example, the very deep caldera lakes researched by Boehrer, Fukuyama, & Chikita (2008). Others are noticing a change in deep water circulation, with shifting surfaces temperatures either making it easier or more difficult to mix the lake (Merchant & Woolway, 2019; Moore, EJ, Smith, & JW, 1996).

Techniques and practices that protect lakes are vital tools for maintaining a healthy balance between ecosystems, agriculture, energy production, and drinking water. The first step to deep lake protection is to gain a full understanding of the deep-water physical processes that govern the resulting chemical and biological processes. The purpose of this thesis is to investigate the natural processes leading to the renewal and circulation of deep, hypolimnetic water within Quesnel Lake, British Columbia, Canada (Figure 3.1.1).

1.1 Statement of the Problem

Quesnel Lake is a deep (>500 m), oligotrophic, fjord-type lake located in the Cariboo Mountain region of British Columbia (BC). The remote, three-armed lake stretches nearly 100 km, with two arms reaching northerly and easterly into the mountains and the third arm spanning west into the Cariboo plateau. The western arm contains a sub-basin, known as the West Basin, where the lake outflows and forms the Quesnel River. The town of Likely, BC is found near the outflow, and the entire Quesnel River Watershed is populated by approximately 20,000 people (Lamont, 1991). The Cariboo Mountain region of British Columbia is a productive logging area and supports several types of mining. Quesnel Lake itself is a popular recreation site for camping, fishing, boating, hiking, wildlife viewing, skiing, and resorting. In addition, Quesnel Lake is one of the largest salmon fisheries in the Fraser River watershed, supporting a multitude of salmon species including sockeye, chinook, kokanee, pink, and coho salmon in addition to an abundant number of other native aquatic species. (Sebastian et al., 2003).

Evidence from decades of field studies indicate that the deepest waters, found in the East Arm of the lake, are well-ventilated (Laval et al., 2012). The mechanism and timing of this regular deep-water renewal is unknown. Research by Thompson (2019) identified and characterized strong winds and storms that frequent the region throughout the year. This was in conjunction with work done by Laval et al. (2008), which found evidence of large exchange flows between the main body of the lake and the West Basin. It was suspected that strong winds from certain storms were responsible for large-scale mixing processes.

In August 2014, the collapse of the Mt Polley Mining Company's tailings pond retention dam led to roughly 20 Mm^3 of tailings, wastewater, and scored overburden to flow into the West Basin of the lake via Hazeltine Creek (Mount Polley Mining Corporation (MPMC), 2015). Monitoring of the waste from the date of the spill until 2 October 2014 showed waste was distributed via settling to the hypolimnion of the West basin, flushing down the Quesnel River, and spreading along the thermocline into the main body of the lake (Petticrew et al., 2015). Research in the intervening years has shown a shallowing of the West Basin by ~10 m, and annual resuspension of waste sediments following a seasonal cycle, with a downward interannual trend. An analysis of the full lake suggests a 10-year period of particle settling and flushing outward through of the Quesnel River is needed to return turbidity in the West Basin back to pre-spill values (Granger, 2020). As of this writing, no remediation has taken place within the lake itself, though Hazeltine Creek has been partially restored (A. Bronsro, Ogilvie, Adams, & Nikl, 2016). A deeper understanding of waste resuspension and distribution throughout the lake is needed to determine what, if any, rehabilitation is possible.

This thesis is a part of the collective investigation into the impact within Quesnel Lake following the Mt Polley Mine spill. Research by Granger (2020), Hamilton (2020) and Petticrew et al. (2015) amongst others, suggest large amounts of the spilled contaminants migrated to the main body of the lake. The researchers have shown that waste settles to the lakebed or is stored in the hypolimnion, where it is prone to resuspension. The main body of the lake has been implicated as source of sediment into the West Basin since the spill.

1.2 Research Questions

The primary purpose of this study is to learn how and when the deep water of Quesnel Lake is renewed. The focus of the research will be within the East Arm of Quesnel Lake, the deepest region of the lake. The study period spans from fall turnover 2006 to spring turnover 2007, with special attention paid to the inverse stratified period between the turnovers. This task will be achieved using a comprehensive data set including meteorological data, and physical and chemical water measurements spanning from summer 2006 to summer 2007, as well as a ten-year data series of temperatures recorded at 500 m from a moored instrument chain in the East Arm of the lake. Using the available data set the following questions are addressed.

1) What natural processes lead to ventilation of the deepest water of Quesnel Lake?
2) When is the deep water of Quesnel Lake ventilated, and with what regularity?
3) What is the impact of deep-water ventilation on homogenization of the water column?
4) What causes the annual trends of increasing and decreasing temperature at 500 m depth during inverse stratification?

Chapter 2: Literature Review

2.1 Description of Deep Fjord-type Lakes

While lakes can form any number of ways, most are formed by runoff within a watershed filling a natural basin. The basins of fjord-type lakes are formed very similarly to marine fjords, hence the name. During periods of glaciation, deep narrow valleys are carved from the underlying mountains. As the glacier melts a lake can form in the valleys if the valley mouth is enclosed behind a moraine berm. Fjord-type lakes are typically much longer than they are wide, and may have multiple arms. They are continually fed through precipitation and snowmelt from the mountains the glacier once flowed through. The berm end of such a lake often becomes the outflow in the form of a river, whose discharge may vary seasonally in accordance to the snow-melt and runoff from the mountains. (Hutter et al., 2011)

Fjord lakes are often the result of overdeepening, which describes when a glacier carves out a basin valley that is deeper than the general level of the ground on which it is flowing (Nasmith, 1962). The average depth of lakes globally was estimated by Cael et al (2017) to be 41.8 m (adjusted from previous estimates 62-151 m (Cael et al, 2017)). In contrast fjord lakes tend to be much deeper. Several fjord lakes found throughout British Columbia are very deep; for example, Quesnel Lake (511 m), Adams Lake (457), Okanagan Lake (232 m), and Harrison Lake (279 m) (BC Geographical Names Office, 2020).

Fjord lakes are found in climates that either previously supported or currently support glaciation. For this reason, most fjord lakes are in cold or temperate climates and will experience a winter and summer stratification as well as two basin-wide mixing events each year. (Gregory, 1913; Syvitsky, Burrell, & Skei, 1987)

2.2 Density of Water

The density of water is dependent upon temperature, pressure, and suspended and dissolved solids (turbidity and salinity) as described by an equation of state (Millero, 2000). Lake waters commonly have a vertical structure due to density variations from each of those state variables. Basin geology, inflows, weather, climate, depth and elevation will all influence density in lakes.

A unique property of liquid water is the nonlinear relationship between density and temperature. Figure 2.2.1 shows the density of pure water at 1 atm as a function of temperature from 0 to 20°C according to the UNESCO (1981) equation of state. The thermal expansion coefficient, α, is a property that explains how molecules expand or contract their volume in accordance with temperature changes, thereby changing their density. The temperature of maximum density (TMD) for pure water at standard atmospheric pressure was estimated at 3.9839 °C by Chen & Millero (1986), and is commonly approximated at 3.98 °C. TMD corresponds with $\alpha = 0$, where α is negative between the temperature of freezing and TMD and positive at water temperatures greater than TMD. Water at TMD is at its heaviest and the warmer or colder a water parcel is compared to TMD, the more buoyant the parcel becomes.

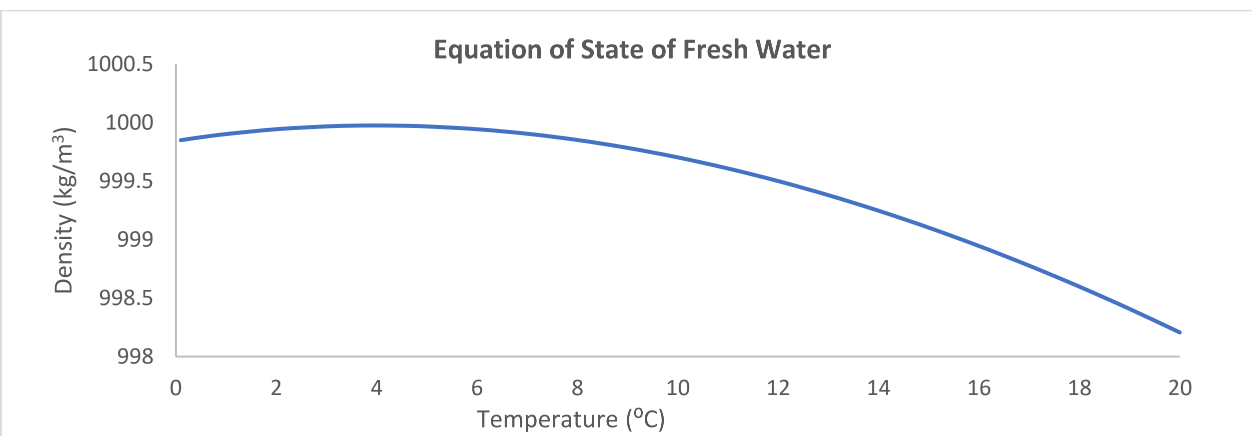

Figure 2.2.1 Graphical representation of the equation of state for the range of liquid water temperatures typically observed in temperate lakes (UNESCO 1981).

Water is slightly compressible, which causes TMD to decrease with depth due to the hydrostatic pressure of the water column. The relationship between TMD and depth (henceforth designated as TMD(z)) is roughly linear and can be approximated as a change of 0.2 °C per 100 m. Often lake research ignores this pressure dependence of TMD. Indeed, these effects are negligible unless a lake is very deep and the water in question is very close (within ~1 °C) to TMD(z). 'Very deep' is hard to quantify, but for the purposes of this work, depths greater than 200 m will be considered our depths of importance. This follows the reasoning of Boehrer & Schultze (2008) that at this depth the difference between in situ density and potential density (the density of a water parcel at standard temperature and pressure (STP)) are of the same order as a weak thermal or salinity stratification typical to lakes. This study's focus is on a very deep lakes (>200 m), meaning the compressibility of water will be taken into consideration

Dissolved and suspended solids also contribute to water density. Increasing dissolved and suspended solids will increase the salinity of water, impacting density (Chen & Millero, 1986). The assumption for many very fresh lakes is that variations in dissolved and suspended solids have negligible impact on density. This study will focus on a freshwater lake with little to no dissolved or suspended solids concentration, meaning that this assumption is considered valid.

2.3 Vertical Stratification

The ratio between kinetic and potential energy in a lake can be evaluated using its vertical structure. Eklund (1965) made a mathematical argument that the most stable stratification a lake could have would be a temperature profile line at ½ the slope of TMD(z). This represents a state of zero kinetic energy, though this profile is rarely seen in nature. The zero potential energy case, as seen during turnover, occurs when the lake is fully mixed (homogeneous). Following homogenization, as structure develops, the potential energy changes accordingly. Increasing potential energy indicates strengthening stratification while increasing kinetic energy represents the break down of stratification due to mixing.

A vertically temperature-stratified lake is traditionally split into three general semi-discrete layers; the epilimnion, metalimnion, and hypolimnion. The epilimnion is the upper most layer of a lake, generally spanning from 0-30 m in depth, and is the most susceptible to atmospheric disturbances. It is the most dynamic part of the lake, often seeing the highest rate of mixing. The metalimnion is a transitional zone between the epilimnion and the deep waters of the lake. The principal feature of this layer is the thermocline. The thermocline is defined as the steepest temperature gradient in the lake. The strength of the thermocline is an indicator of the strength of stratification of the lake and a strong thermocline will inhibit the top and bottom waters from mixing. The hypolimnion of a thermally stratified lake is the water below the base of the metalimnion. In deep lakes, the hypolimnion may well contain the majority of the volume of the lake. While the hypolimnion can be considered homogenous when compared to the epilimnion, slight gradients contribute to rather interesting mixing events. (Hutchinson & Loffler, 1956; Hutter et al., 2011; Imboden & Wuest, 1995).

The complete seasonal homogenization of lake water from top to bottom is referred to as turnover. Turnover is an important process in lakes and will be discussed further in section 2.3.1. Seasonal temperature stratification and turnover patterns are often used as a lake classification scheme, with the standard set by Hutchinson & Loffler in their 1956 paper that estimated a lake's thermal stratification type by its elevation and latitude. While some lakes are permanently stratified (amictic), some lakes turnover continuously (polymictic). The focus of this research is on dimictic lakes, which have two turnover events each year, typically during fall and spring, separated by regular stratification in summer and inverse stratification over winter.

2.3.1 Stratification Due to Temperature

Because water has a temperature of maximum density at around 4 °C, within the span of its liquid phase, it has two types of vertical temperature stratification: summertime stratification (often just referred to as stratification), and winter or inverse stratification. At all times in a stable thermally stratified lake, water closest to TMD(z) will be found toward the lake bottom with buoyant water above it. The buoyant water may be warmer or colder than TMD.

During summer stratification temperature increases toward the surface. In the summer, dimictic lakes have a warm epilimnion floating on top of a cold hypolimnion separated by a metalimnion containing steep temperature gradients and a strong thermocline. Generally, water above and below the thermocline will be unable to intermix.

In the winter, inverse stratification occurs. Surface water will be at or below TMD(z), *decreasing* in temperature moving toward the surface. Very deep lakes will have a temperature maximum in the metalimnion, sometimes referred to as the meso-temperature maximum (Bouffard & Wüest, 2019; Carmack & Weiss, 1991). Additionally, the metalimnetic water can be at its in-situ temperature of maximum density. This is called the compensation depth and will be described more in section 2.3.2. The compensation depth and meso-temperature maximum will sometimes correspond but are separate entities. The wintertime metalimnetic features will prevent free mixing of epilimnetic and hypolimnetic water.

Turnover events in dimictic lakes involve surface warming through the spring and surface cooling through the fall, bringing the temperature of the epilimnion closer to TMD.

This will weaken and destabilize stratification in the water column, creating kinetic energy and decreasing the potential energy. Gravity, wind, or other forces push heavy, denser water downward, creating turbulence and mixing which homogenize the water column. These forces will be discussed in detail in section 2.4.

2.3.2 Stratification Due to the Effects of Pressure on TMD

Very deep lakes are capable of stratifying due to the impact pressure effects have on TMD. This is known as thermobaric stratification (McDougall, 1987) and has been well documented in many deep lakes such as Lake Baikal (Russia), Babine Lake (Canada), Crater Lake (USA), Kuttarako (Japan), Shikotsuko (Japan), and Tinnsjø (Norway). This process is most often observed in the hypolimnion due to the relatively high hydrostatic pressure of the water column, and the isolation of this water from direct forcing from the atmosphere (Farmer & Carmack, 1981). The change of water density with pressure means that a lake will be statically stable, while having a temperature versus depth profile with a gradient of up to approximately -0.021 °C bar^{-1} (Eklund, 1965). In deep lakes without salinity gradients, pressure effects can be the sole source of stratification, as hypolimnetic water is often relatively homogenous in temperature.

Deep inversely stratified lakes have an important depth known as the compensation depth. The compensation depth is where the in-situ temperature of the water is equal to the in-situ TMD(z) (Boehrer & Schultze, 2008; Carmack et al., 1991; Piccolroaz & Toffolon, 2013) and where α goes to zero as was described in section 2.2. This means water both above and below this depth will decrease in temperature, making the compensation depth the temperature maximum of the water column if it is statically stable. The compensation depth, like the thermocline, acts as a barrier between the epilimnion and the hypolimnion intermixing.

If buoyant surface water is displaced downward to a depth at or past the compensation depth, where its temperature is equivalent to or cooler than the in-situ TMD(z), the surface water may remain at this displacement depth if equal in temperature to the local TMD(z), or it may continue sinking to a depth of neutral buoyancy. This unique phenomenon is called a thermobaric instability as was described in Lake Baikal by Carmack & Weiss (1991).

Figure 2.3.1 is a conceptual diagram for the creation of a thermobaric instability. Panel (a) shows a stable, inversely stratified temperature profile. The slope of the profile is negative above where the profile crosses the TMD(z) line, and the temperature is homogenous below the TMD(z) line. In panel (b), an external force has displaced the temperature profile downward by ΔDepth, pushing the knee of the profile below the TMD(z) line. The negative sloped region of this profile is now unstable because water closer to the TMD(z) is now above water that is further from the TMD(z). This will trigger a thermobaric instability. Panel (c) displays the result of this progression. Forcing has ceased and a thermobaric instability has occurred. The thermobarically unstable plume of water has sunk to a point of neutral buoyancy, mixing and cooling the water along the way by ΔTemperature. The positive slope of the bottom water is equal to or greater than the slope of TMD(z). This means all water is of equal or lesser density if moving from the bottom vertically upward and the profile is stable. The knee has returned to a position above the TMD line, so it also has a stable slope.

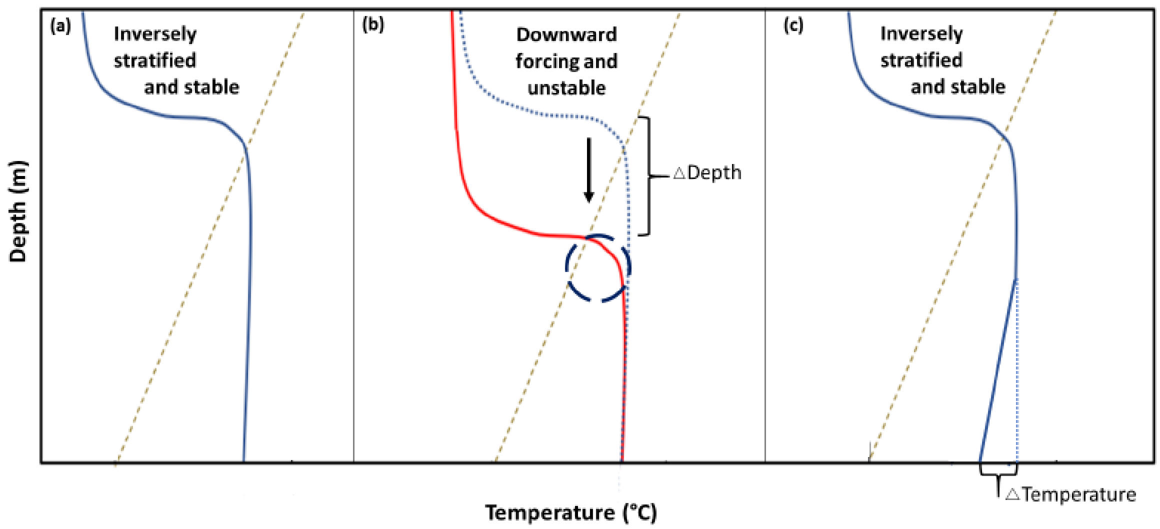

Figure 2.3.1 Theoretical schematic of a thermobaric instability. (a) A stable temperature profile (solid line) crossing through the TMD profile (dashed line). (b) Forcing displaces the temperature profile (blue dotted line) downward (red line) and the "knee" (circle) across the TMD profile, becoming unstable and initiating a thermobaric instability. (c) Forcing has ceased and the profile returns to its original position. The profile has stabilized and the bottom water has cooled from the thermobaric plume.

The direction in which a displaced water parcel moves in an inversely stratified lake is dependent on its position relative to the compensation depth. α changes sign on either side of the compensation depth. Thermobaric instabilities will only occur when a parcel of water crosses the compensation depth and changes from positively buoyant to negatively buoyant. A displaced water parcel that does not cross the compensation depth will return to its original position once forcing ceases (if mixing is ignored).

2.3.3 Mixed Layers and Turnover

During open water periods, most lakes will experience the majority of forcing at the air/water interface. Interactions here create an active and dynamic layer referred to as the convective or surface mixed layer. The surface mixed layer is often used as a proxy to track and predict changes within the rest of the lake. Often the surface mixed layer and epilimnion are regarded as one in the same; however, the surface mixed layer can be differentiated from the epilimnion in its volatility. Where the epilimnion is regarded as a seasonal layer, the surface mixed layer changes on time scales correlating with forcing (Imberger & Jul, 2007; Bouffard & Wüest, 2019; Farmer & Carmack, 1981; Imboden & Wuest, 1995).

Special attention is drawn to the surface mixed layer in order to quantify turnover for this study. Methods to predict turnover vary between researchers, but essentially turnover is defined as homogenization of the water column. If the surface mixed layer is defined as the homogenous layer beginning from the surface and continuing to a depth where stratification exists, then a surface mixed layer extending through the entire depth of a lake represents a fully turned over lake. In order for the water column to homogenize in deep lakes after inverse stratification (i.e. spring turnover), the surface mixed layer must be energetic enough to break down temperature stratification in the thermocline and overcome buoyant forces at the compensation depth. At the surface this energy is provided by wind forcing and heat driven convection.

The bottom mixed layer, also known as the nepheloid layer or benthic boundary layer, is formed from diffusion and shearing at the water sediment interface (Gloor, Wüest, & Münnich, 1994; Lorke & MacIntyre, 2009). Shearing is produced by any internal waves or currents that produce a horizontal bottom velocity. This kinetic energy is dissipated by turbulence, causing resuspension of sediments into the water column. The exact definition of this layer is vague and varied from discipline to discipline, but it can be defined similarly to the surface mixed layer. The layer is largely homogenous in density (i.e. salinity and temperature). Oceanographers have measured the layer using temperature thresholds and find the layer thickness is on an order of tens to thousands of meters (Huang (2019); Lozovatsky & Shapovalov (2012)). In lakes the layer thickness is on the order of 1 – 100 m, dependent on the researcher and the research. The bottom mixed layer has received less focus in comparison with the surface mixed layer; however, research by Crawford and Collier (2007) in Crator Lake, Gloor et al. in Lake Baikal, and Granger (2020) in Quesnel Lake have drawn attention to the importance of bottom water mechanics.

2.4 Lake Forcing

Lake forcing drives the cycles of stratification and turnover in lakes and describes any force exerted on lake waters that creates kinetic energy. Kinetic energy in lakes can be split into non-turbulent (i.e. large scale, coherent) flow and turbulent kinetic energy (TKE). TKE enhances mixing and is produced through shear production and gravitational convection (a.k.a. buoyant production). TKE will not be directly addressed here; rather, its energy sources are evaluated. These are predominantly thermal forcing and wind energy.

Thermal forcing at the lake surface is regarded as the most influential in lakes and has historically been a key factor in lake classification (Lewis Jr., 1983). Thermal forcing in lakes manifests due to the dependence of water density on temperature, creating stratification or driving convection. Wind forcing is also very influential for certain lakes and has been investigated extensively (Farmer & Carmack, 1981; Gloor et al., 1994; Laval et al., 2008). Other forcings such as inflow and outflow, or geothermal activity can also be strong components in lake mixing but will not be addressed in this review as this study focuses on thermal and wind forcing.

Lake forcing has traditionally been quantified using several mathematical methods, including heat budgets and buoyancy flux, wind forcing and shear, and wave theory. Researchers compare the magnitudes of various forcings to one another to assess how lake structure is impacted.

2.4.1 Heat Budget

Heat budgets are a method used to track how a body of water gains or loses heat energy from its surroundings. The heat contained by the water body is referred to as the heat content while the incoming and outgoing fluxes are called the heat fluxes. Finding the balance between a lake's heat content and the net fluxes shows the general magnitude of each flux and provides an overall estimate of the error in the magnitude of each flux. A complete heat budget displays the importance of heat energy in the seasonal energy cycle of a lake.

The heat content of a lake will cross a zero when its average temperature crosses a reference temperature. Often 4°C is used as the reference temperature, applying the concept that turnover occurs when a lake homogenizes to TMD. If this method is used a lake will have positive heat during the summer stratified season, zero heat at fall turnover, negative heat over winter stratification, and zero heat at spring turnover.

Heat exchange primarily takes place at the air/water interface. Heat is then distributed through the water column in various ways such as direct penetrating shortwave radiation, convection currents, wind mixing, or diffusion. A heat budget for a lake is given by S.W. Hosteler:

$$\boldsymbol{\frac{dH}{dt} = \pm Q_{in} \pm Q_{out} + (1 - \alpha_S)SW + (1 - \alpha_L)LW - Hs - Hl} \qquad \text{(Eq. 2-1)}$$

where $\frac{dH}{dt}$ is the change in total heat of the lake over time, Q_{in} and Q_{out} are the inflow and outflow respectively, α_S is the shortwave albedo of the surface, α_L is the longwave albedo of the surface, SW is shortwave, LW is longwave, Hs is sensible heat, and Hl is the latent heat of vaporization. A visual representation of these fluxes can be seen in Figure 2.4.1.

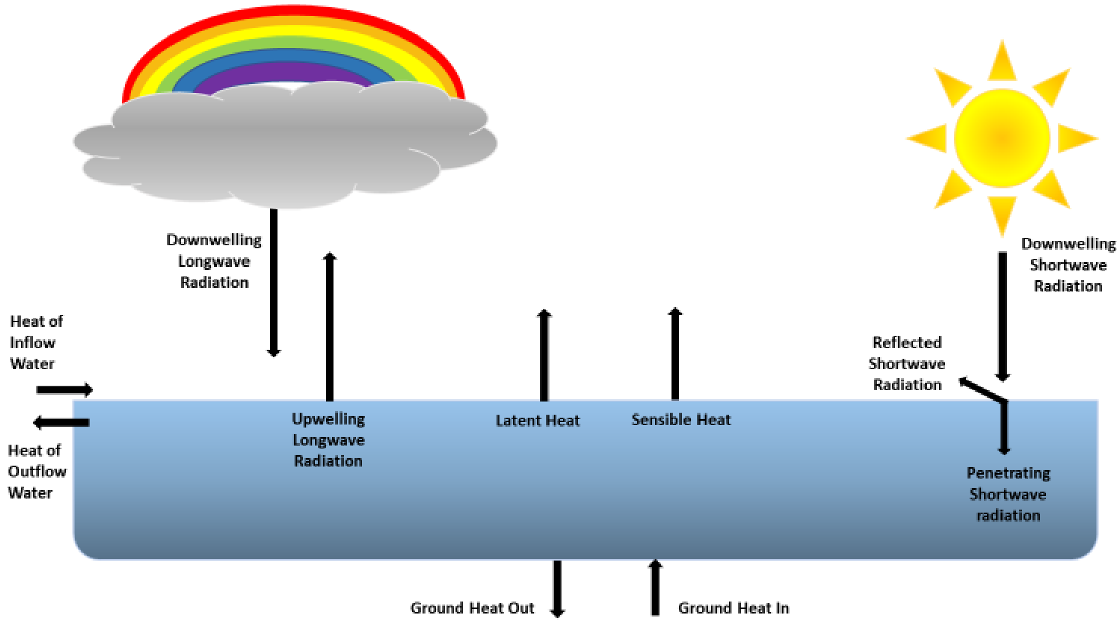

Figure 2.4.1 A representation of the heat fluxes impacting a water body.

2.4.2 Buoyancy Flux

Buoyancy flux describes the rate of change of potential energy in a lake (Imboden & Wuest, 1995). The buoyancy of a volume of water is determined by the difference between its density and the surrounding ambient density. This is the driving force of convection (Bouffard & Wüest, 2019) and determines whether a water parcel will sink, raise, or remain at its position. The breaking down of stratification through a change in buoyancy will lead to convection. In inversely stratified lakes, the buoyancy of a parcel of water approaches zero as its compensation depth is reached, whether from above or below.

The surface buoyancy flux, B_0, neglecting salinity or suspended particles, can be written as

$$\boldsymbol{B_0} = \frac{\boldsymbol{g}}{\rho}\left(\frac{\boldsymbol{\alpha}}{\boldsymbol{c_p}}\boldsymbol{H_Q}\right) \qquad \text{(Eq. 2-2)}$$

where g is acceleration due to gravity, α is the thermal expansion coefficient of water, ρ is the density of the water surface, c_p is the specific heat capacity of water ($4.18\text{x}10^3$ J kg^{-1} °C^{-1}),

H_Q is the net surface heat flux. Eq. 2-2 shows that in its simplified form, buoyancy flux at the air/water interface is dependent on the heat fluxes at the surface. If buoyancy flux is positive, convection is actively deepening the surface mixed layer. If buoyancy flux is negative, the forces are stratifying the layer. (Bouffard & Wüest, 2019; Imboden & Wuest, 1995)

2.4.3 Wind Mixing (surface)

Wind causes transport and mixing in lakes. Transport is brought about by wind-generated currents or by wind-induced waves producing vertical motion. Mixing occurs due to shear-induced waves and turbulence. Strong winds are often the largest source of kinetic energy in a lake (Imboden & Wuest, 1995), and the greater the fetch of a lake the more influential this energy can be. The epilimnion is continuously subject to wind forcing, as the interface is in direct contact with the atmosphere (even under ice, though to a lesser degree). Wind forcing at the surface also has potential to induce shear and mixing at the thermocline, the lake bottom, and other density interfaces.

Wind shear velocity, u_* is a velocity scale for the shear stress exerted by wind at the lake surface (Farmer & Carmack, 1981; Hutter et al., 2011). Wind shear velocity is defined as

$$\boldsymbol{u_* = (\tau/\rho_0)^{1/2}} \tag{Eq. 2-3}$$

Where ρ_0 is a reference density and wind stress, τ, can be estimated empirically as

$$\boldsymbol{\tau = C_d\, \rho_{air}\, u^2} \tag{Eq. 2-4}$$

where C_d is a drag coefficient, ρ_{air} the density of air, and u^2 is the square of the wind speed.

A comparison of the magnitude of wind power and buoyancy flux lends insight into which forcing is dominating the structure of the surface mixed layer (Farmer & Carmack, 1981). If the two forcings are in opposition with a negative (stabilizing) B_0, wind shear, even under strong wind conditions, may have little impact on mixing. Conversely, if B_0 is very weakly negative or slightly positive, even small amounts of wind shear can cause significant mixing.

The Monin-Obukov length (L_{MO}) is a parameter that determines the relative influence of buoyancy and wind. When buoyancy flux is positive (unstable), the L_{MO} specifies the depth within the surface mixed layer to which wind induced mixing dominates over convective mixing. Any mixing beyond this depth is dominated by convection.

$$\boldsymbol{L_{MO} = \frac{{u_*}^3}{kB_0}} \qquad \text{(Eq. 2-5)}$$

where $k \approx 0.41$ is the Van Kármán constant.

2.4.4 Seiche

Mixing below the surface layer is typically the result of shear production due to baroclinic motions forced by wind set up. Wind can force epilimnetic water downwind, setting up a baroclinic pressure gradient across the lake, the relaxation of which leads to shearing and mixing at density interfaces and the bottom boundary. If the wind forcing is greater than the stability of the stratification, the thermocline can tilt enough to bring hypolimnetic waters to the surface at the upwind end of the lake. At this point the dense water is exposed to the wind, aiding the mixing process. The opposite occurs at the downwind end of the lake, whereby epilimnetic or metalimnetic water is forced downward, possibly initiating a thermobaric instability (2.3.2). This is called upwelling and downwelling respectively, and can be predicted by the Webberburn number

$$\boldsymbol{W = \frac{g' h_1^2}{u_*^2 L} < 1} \qquad \text{(Eq. 2-6)}$$

where h_1 is the change of height of the water surface, L is the length of the basin, and g' is the reduced gravity given by $g' = \frac{\rho_1 - \rho_2}{\rho_0}$ with ρ_1 and ρ_2 being the density of the first and second layer. Figure 2.4.2 show the tilt of the thermocline and the upwelling condition, respectively.

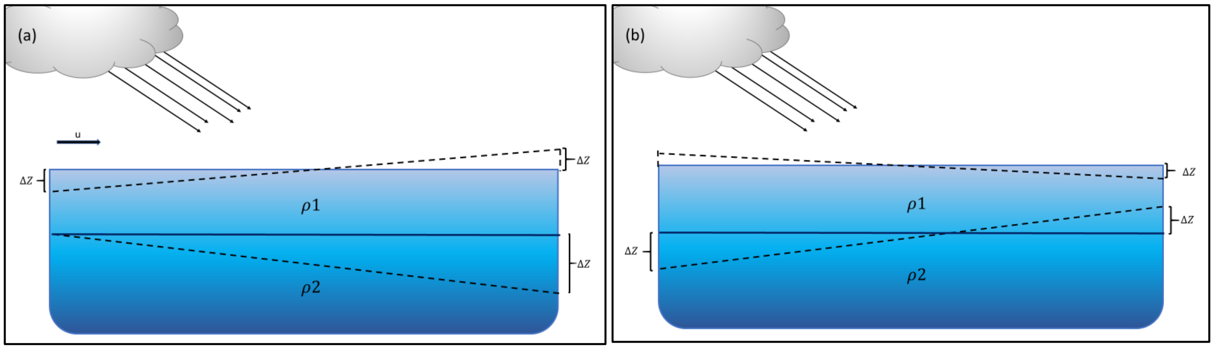

Figure 2.4.2 A representation of wind setup leading to seiching. Where dashed lines represent the change in slope of the water interface. (a) Deflection of the thermocline in a stratified lake due to wind set up. (b) The response of the layers once wind forcing has stopped, and momentum has caused the water body to overshoot the point of gravitation stability, creating an oscillation.

Once the forcing that creates the set up is removed, the lake will try to restore itself to a gravitationally stable position. This creates an oscillatory motion known as a seiche (Figure 2.4.2) and was observed as early as 1876 (Imboden & Wuest, 1995). Seiches are standing waves along an interface that run the entire length of a stratified region (Hutter et al., 2011; Imboden & Wuest, 1995). The period of these waves can be found using Merian's formula

$$\boldsymbol{T} = \frac{\boldsymbol{2L}}{\boldsymbol{n}(\boldsymbol{g'H_{eff}})^{\frac{1}{2}}} \qquad \text{(Eq. 2-7)}$$

where L is the length of the basin, n is the number of horizontal modes, and H_{eff} is the effective height if the system has more than a single layer, and is given by

$$\boldsymbol{H_{eff}} = \frac{\boldsymbol{h_1 * h}}{\boldsymbol{h_1 + h_2}} \qquad \text{(Eq. 2-9)}$$

If a system is composed of only a single layer $H_{eff} = H =$ the depth of the basin. The wind duration needed to create a seiche can be estimated using the quarter period, i.e. T/4 (Stevens & Lawrence, 1997).

2.5 Summary

This thesis will build on the ideas of previous researchers to identify the physical drivers of deep-water mixing and renewal in Quesnel Lake. Thermal and wind forcing will be analyzed using the theory described in this section and the methods described in Chapter 3 to explain these processes.

Chapter 3: Methods

Field data collected over the winter of 2006 – 2007 at Quesnel Lake were analyzed to investigate wintertime deep-water ventilation events in the East Arm of the lake. A heat budget was developed to validate surface heat flux calculated from meteorological data. The estimate of surface heat flux was then used to calculate a surface buoyancy flux, allowing for analysis of surface layer mixing and convection. Buoyancy flux was compared with wind power at the water surface computed from wind data collected at field weather stations. Wind forcing was also compared to prior research to identify periods of wind sufficient to initiate seiche. Vertical water temperature profiles were analyzed in space and time to identify seiche events, mixing, and thermobaric instabilities. The thermistor record and the surface forcing were then compared to identify trends of warming and cooling at the deepest point in the lake, indicating ventilation.

3.1 Site Description

Quesnel Lake is a very deep, dimictic, fjord-type lake in a temperate climate zone in the Cariboo Mountains of British Columbia, Canada as shown in Figure 3.1.1. The lake is thermobarically stratified, with a maximum known depth of 511 m (Laval et al., 2008), making it the 13th deepest lake in the world. The lake has three narrow arms with a 100 km thalweg and a maximum depth of 511 m. There are 3 major inflowing rivers, numerous smaller inflowing creeks, and one major outflow. The volume of the entire lake is estimated as 41.8 km^3 and average residence time of the lake is estimated to be 10.1 years. (Laval et al., 2008).

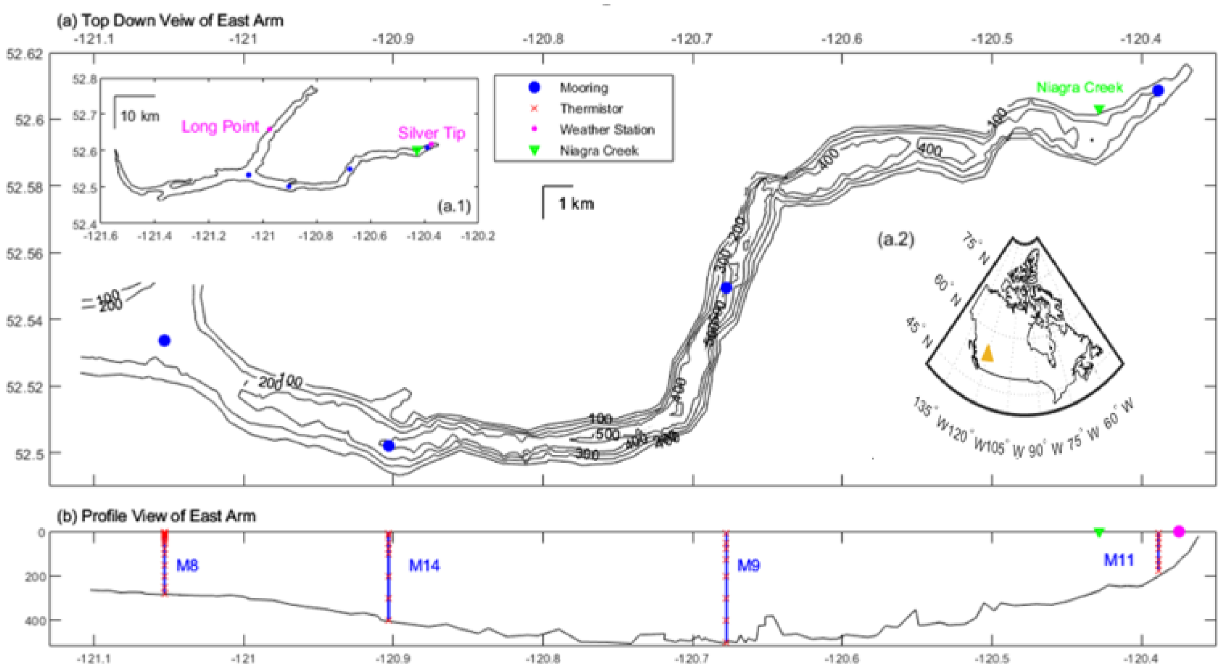

Figure 3.1.1 Map of Quesnel Lake. (a) The main panel displays a bathymetric map of the East Arm of Quesnel Lake in the Cariboo Mountain region of British Columbia, Canada (a.2). The blue dots on the bathymetry map indicate the location of four moorings that were in place during the study period. (a.1) Location of the moorings and lake-based weather stations used in this study. (b) Profile view of the East Arm bathometry, where red x's mark the depth of thermistors on each mooring chain.

For this work, the East Arm was defined as the lake section from the eastern tip of Quesnel Lake to the junction of the three lake arms, at mooring M8 (Figure 3.1.1). The thalweg length between M8 at the junction to the eastern tip is roughly 50 km and the average arm width (surface area divided by thalweg length) is 1 km. The East Arm is the longest and deepest arm of the lake and extends from mid lake into the Cariboo Mountains. The deepest point of the entire lake is found here near mooring M9, at 511 m. In Figure 3.1.1 the locations of the moorings (and depths) of the East Arm from west to east are M8 (283 m), M14 (400 m), M9 (500 m), and M11 (175 m). Niagara Creek is the only major inflow in the East Arm and enters the lake on the northern side of the eastern tip, near M11. Despite winter at Quesnel

Lake being very cold (average air temperature during inverse stratification 2006-2007 was -0.18°) the arm rarely freezes beyond shore ice and ice at the easternmost tip.

The wind climatology of Quesnel Lake was recently analyzed by Thompson (2019). Quesnel Lake lies in a transitional climate within the Interior Plateau in the Cariboo Mountain Region of Northern British Columbia. The wetter Coast Mountains lie toward the west and the drier Rocky Mountains to the east. Winds in this region are generally categorized as prevailing westerlies as is typical of the mid-latitudes of the northern-hemisphere (Sharma & Déry, 2016). October to May winds in the region are above average for the region. In his local climatological research of synoptics winds of the Quesnel Lake region, Thompson found that the strongest winds tend from the South Southeast.

3.2 Field Data Collection

Quesnel Lake has been studied by various researchers and organizations for decades. These groups include University of British Columbia (UBC), The Institute of Ocean Science (IOS), University of Northern British Columbia (UNBC), and the Department of Fisheries and Oceans (DFO) amongst others. Research has been conducted on physical and biological aspects of the lake with primary objectives of improving salmon habitat and understanding the mechanics of very deep lakes. The data presented here was collected predominantly by UBC and IOS between 2006 and 2007.

3.2.1 CTD Data

Conductivity, Temperate, and Depth (CTD) measurements taken over three separate field campaigns between fall 2006 and spring 2007 were processed to show ventilation of deep water over winter. The CTD used in these campaigns was a Seabird 19v2+ with an addition dissolved oxygen sensor. Temperature, dissolved oxygen (DO), and conductivity data were smoothed using a 12.5 s moving average and were compared to assess the vertical structure throughout the year. CTD casts taken at locations closest to each mooring chain were chosen for analysis. Dissolved oxygen was chosen to be reported in units of mg L^{-1} instead of as a percentage saturation to remove the effect of temperature in different times of the year. Water samples were not taken along with CTD measurements and DO sensors were not checked for drift. An analysis of conductivity showed that variance with depth and time was negligible. Salinity of the water over the three CTD campaigns varied between 0.085 g kg^{-1} and 0.089 g kg^{-1}, with a vertical trend from top to bottom (Figure 3.2.1). The values were depth-averaged, and a salinity of 0.087 g kg^{-1} was chosen to represent the full water column at all times of year.

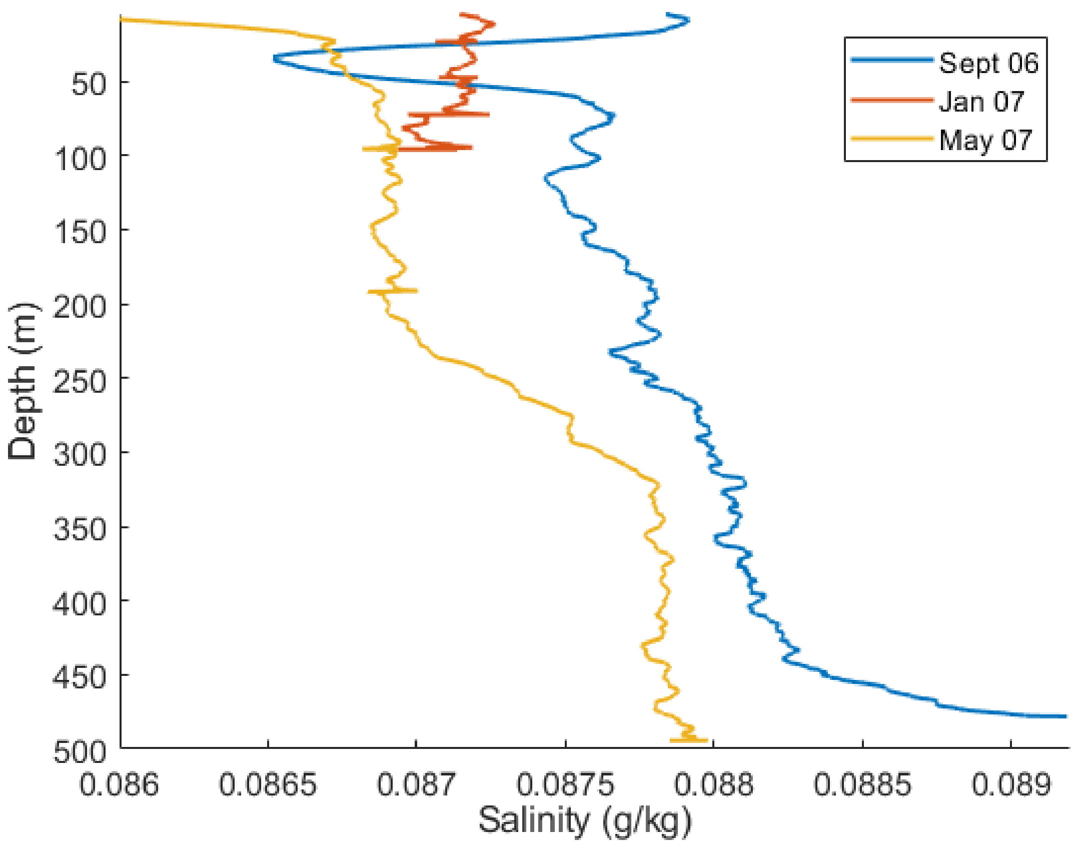

Figure 3.2.1 Salinity profiles taken at M9 over the study period. The January profile was not taken to the full depth of the lake.

3.2.2 Moorings

From October 2006 to October 2007, eight mooring chains, each holding varying numbers of thermistors, were deployed in Quesnel Lake. The moorings consisted of an anchor, a rope of appropriate length, and a sub-surface float situated approximately 5 m below the surface. The thermistors were RBR TR-1050s with an accuracy of 0.002 °C. For the analysis in this thesis, only the moorings M14, M9, and M11 will be referred to in detail. These moorings were located along the thalweg through the East Arm. Moorings were serviced prior to each deployment annually. Servicing included changing batteries and desiccant packs and clearing the logger memory to guarantee space for new data.

3.2.3 Weather Stations

Weather data over the study period was obtained from local shoreline weather stations, the Williams Lake Airport, and modelled data from the National Renewable Energy Lab (NREL). Over the 2006-2008 period, three weather stations were located on the shores of Quesnel Lake. Of these, the Long Point and Silver Tip stations, as well as a thermometer and relative humidity (RH) probe mounted on M8 were used in this analysis. The shoreline weather stations were produced by Onset Corporation and comprised of varying configurations of anemometers, thermometers, barometers, RH meters, wind directional devices, and incoming solar radiation gauges. The anemometers of the Long Point and Silver Tip Stations were mounted at 7.5 m. The data gathered from the Williams Lake Airport were obtained from their historical weather data database (Government of Canada) and used to fill gaps in the wind record. Modeled solar radiation data was provided by NREL and used to estimate this parameter during gaps. Data was downloaded from their online National Renewable Energy Labority Database (NSRDB) (NREL, 2019) from a location equivalent to the M8 mooring.

3.3 Data Processing

Raw field data was converted from downloaded files into MATLAB and processed utilizing the Air-Sea Toolbox v2 (Pawlowicz, 2001) and Gibbs Sea Water (GSW) Oceanographic Toolbox v3 (R2012a). The data was daily averaged to remove diurnal signals, as the study focused on week- and month-long timescales. Exceptions to this include wind direction, which was not smoothed, and wind speed which was averaged either by 30-minute, 1 day, or 36 hours dependent of its use as described in this chapter.

3.3.1 Water Data

Data downloaded from each East Arm thermistor were daily averaged and linearly interpolated in depth to 1 m intervals. The shallowest thermistor of each mooring was located 5 m below the water surface, and water above 5m depth was assumed to be homogenous at the temperature of that thermistor. Data from M14, M9 and M11 were horizontally interpolated over a 1 km scale for the purpose of viewing horizontal gradients.

The temperature of maximum density is an important parameter for this work. To find TMD at depth, the *gsw_t_maxdensity_exact* function was used from the MATLAB GWS toolbox, using salinity constant at 0.087 g kg^{-1} (as outlined in 3.2.1 above) and pressure in decibars. The compensation depth over winter was computed as the intersection depth of the TMD profile and time varying, depth-interpolated temperature profiles.

Mixed layer thickness was determined using a temperature threshold. The surface mixed layer depth was taken downward from the surface till the greatest depth where the interpolated temperature did not exceed a threshold of 0.05 °C. Likewise, the bottom mixed layer thickness was taken as the vertical distance from the lake bottom to the depth where temperature difference between the 500 m thermistor (taken as representative of bottom temperature) and the vertically interpolated temperature profile was within 0.02 °C. In order to account for the degree of temperature variation in the epilimnion versus the hypolimnion, different threshold values were selected to define each of the surface and bottom mixed layers. Hypolimnetic waters tend to be quite homogenous, meaning that too large a threshold would make the results meaningless. The bottom threshold of 0.02 °C was chosen as it clearly identified trends of the bottom waters in response to wind events.

Seasonal turnover in lakes can be defined using several different methods. In this study, turnover was selected as the date when the surface mixed layer reached its maximum depth while surface buoyancy flux remained positive and destabilizing. This is similar to observations made by (Farmer & Carmack, 1981) while examining summer versus winter stratification in Lake Babine. This method was chosen because the extreme depth of the lake means there is not always a seasonal homogenization of lake temperature over the entire water column. Also, storms passing through the area over the turnover period cause the water to mix, restratify, and mix again. Choosing the maximum depth of the surface mixed layer while buoyancy flux remains positive gave an unambiguous method for choosing an exact date of turnover.

3.3.2 Weather Data

Weather data was used to calculate surface heat flux using bulk formulations from the Air-Sea Toolbox. The weather data used to estimate heat flux were daily averaged to be consistent with the calculated heat content of Quesnel Lake (section 3.4.1). To assess wind shear on the water surface, wind speed was averaged to 30-minute values in order to remove gusts. To isolate wind events capable of causing seiche wind speed was smoothed using a 36-hour moving average. This was consistent with the methods of Thompson (2019).

Not all stations had a full set of meteorological sensors and there were several data gaps in the record due to servicing, weather, or equipment failure. Data from different stations therefore had to be pieced together in order to create a full meteorological picture. Temperature, wind speed, and relative humidity were averaged from all weather stations, while barometric pressure and incoming solar radiation were available only from Silver Tip station.

Incoming solar radiation was only tracked at the Silver Tip station and there are several data gaps through key periods. Data available from the NREL NSRDB was used to fill these gaps. Modelled data were downloaded for Quesnel Lake for the years 2006 and 2007. The NREL data were averaged using the same approach as the Silver Tip weather station radiation data and used to patch the missing time periods. The modelled data fit well with existing data and is assumed to be correct (Figure 3.3.1).

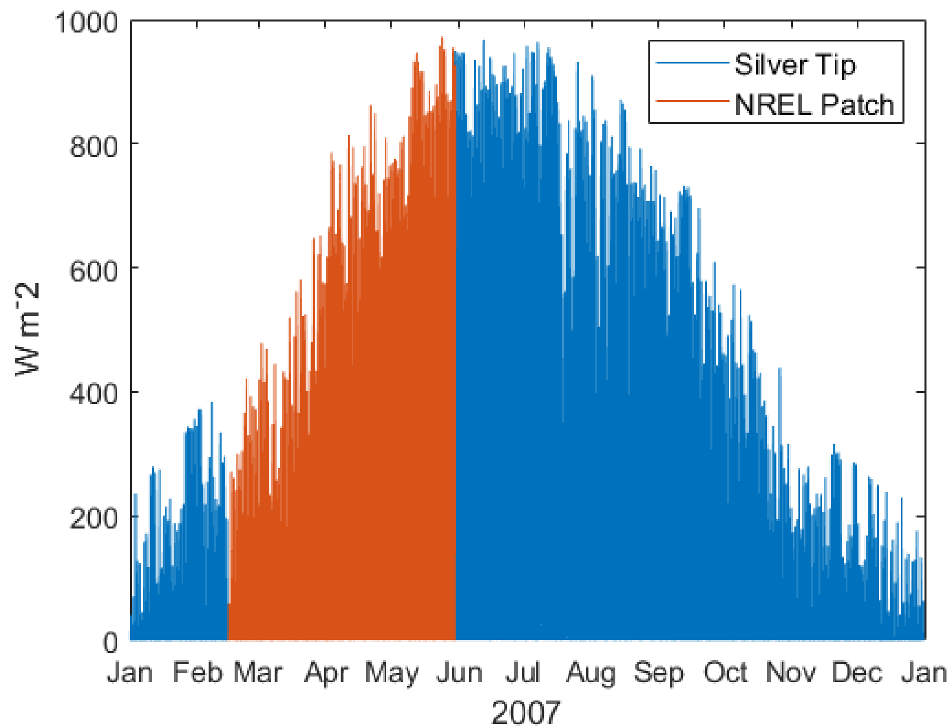

Figure 3.3.1 Radiation data used in completing the heat budget. An equipment failure created a data gap in radiation data at Silver Tip. The NREL data (red), selected from a location equivalent to M8, fit the trends of the data at Silver Tip throughout the year, and was used to fill the gap.

From 22 November 2006 to 06 December 2006, a large data gap was seen in all lakeside weather station anemometers. This is likely due to the anemometers freezing in place. The data was patched with Williams Lake Airport data. This weather station, being situated in the Central Plateau region to the west of Quesnel Lake, will record higher wind speeds than a lakeside anemometer. For this reason, the data should be read and interpreted carefully. While this data is presented in this thesis, the patched event was prior to the wintertime focus of this study, and therefore will not impact the results.

3.4 Data Analysis

Data was analysed to search for correlation between atmospheric forcing and the cooling events witnessed at the bottom of M9. To do so the following steps were taken. A heat budget was created for the East Arm. Surface buoyancy flux was compared to wind power. Wind data was analysed for conditions necessary to create seiche. Horizontal gradients in isotherms seen in moored thermistor data was used to estimate seiche periods. Temperature readings from moored thermistors were used to track changes in mixed layer thickness over time, which was compared to wind data. Bottom mixed layer thickness and the depth of the temperature maximum were compared to periods of warming and cooling at 500 m. Details of each of these steps are outlined below.

3.4.1 Heat Budget

A hypsometric curve was made of the East Arm. The bathymetric data were gathered by the Institute of Ocean Sciences (IOS) in 2001 using a sub-bottom acoustic survey (Gilbert & Desloges, 2012). The hypsometric curve and temperature profiles from each mooring were integrated to create a heat content time series (Figure 4.2.1) of the arm. The heat content was found using the daily averaged, 1 m interpolated temperature data set described in section 3.3.1. The measured temperature profile was assumed to be horizontally homogenous across the arm, and the total heat of the lake was found using:

$$\boldsymbol{H_{content} = c_p \sum_{z=1}^{z_{max}} \rho(z)(T(z) - T_0)A(z)dz} \quad \text{(Eq. 3-1)}$$

where c_p is the specific heat capacity of water (4.18×10^3 J kg^{-1} °C $^{-1}$), $\rho(z)$ is the density of water at depth z, z_{max} is the total depth of the lake, $T(z)$ is the temperature of each layer estimated from the thermistors, and T_0 is the reference temperature, taken to be 3.98 °C (i.e. TMD at the lake surface). A heat content time series was found for each mooring (M14, M9, and M11). As the moorings all reported similar trends, M9 was chosen as representative of the East Arm, as it was located mid-arm and extended the full depth of the lake.

Weather data over the lake was used to create a surface heat flux time series for the study period using the *hfbulktc* function in the MATLAB Air-Sea Toolbox where the input parameters were determined as shown in 3.3.2 The program auto corrects wind speed measurements to 10 m for calculations. The calculated heat fluxes were integrated in time and compared with calculated lake heat content as a validation of the calculated heat flux as described by **Eq. 2-1** in section 2.4.1.

3.4.2 Surface Buoyancy Flux vs. Wind Power

It was assumed that Quesnel lake had negligible salinity and suspended solids based on previous CTD casts. This justified the use of the simplified surface buoyancy flux **(Eq. 2-2)** as described in section 2.4.2. The thermal expansion coefficient, α, and water surface density ρ, were derived using temperature from the shallowest thermistor at M9 and were calculated using the GSW Matlab toolbox.

Wind shear velocity, u_*, was defined using **(Eq. 2-3**) with τ defined by **(Eq. 2-4**). The drag coefficient, $C_{d,}$ was set at 1×10^{-3}, ρ_{air} to 1.25 kg m^{-3}, and u was the 30-minute averaged wind speed measured at 7.5 m above the lake surface.

Surface mixing due to wind shear was compared to convective mixing from surface buoyancy flux utilizing the relation made by the Monin-Obukhov length (**Eq. 2-5**). The resultant values were plotted separately for ease of viewing in Figure 4.3.1.

3.4.3 Seiche Period

Research conducted by Brenner (2017) indicated the possibility of a seiche node in the East Arm at approximately the location of M9. This validated the use of the M14, M9, and M11 moorings to search for tilts in the isotherms that could lead to thermobaric instability.

To assess the deep-water reaction to surface events, significant surface events needed to be isolated, meaning sustained wind events lasting for the quarter period of the fundamental seiche period of the lake. Thompson (2019) conducted research to identify storm types most likely to excite seiche within the arms of Quesnel Lake. His research was based on earlier research by Laval (2008). Laval had calculated the full basin fundamental seiche period of the lake during summer stratification to be 6 days, thus having a 36-hour quarter period. This study replicated Thompson's processes to link these observed storm events to actual seiche events from thermistor data. Though a winter stratification would have a longer seiche period, the 36-hour quarter period was considered a baseline value for the storm isolation process.

Multi-day spikes in wind speed were isolated using a threshold value of wind speed above the 90^{th} percentile for the year of data used in this study. It was observed that these large events, displaying dramatic change in temperature and high wind speed, tended to blow out of the SSE wind direction between 160-180°. Thompson found the same result for major storms over winter, with this wind direction being indicative of mid-winter mid-latitude low pressure systems likely originating in the Gulf of Alaska. Thompson observed these winds were within the 80^{th} percentile of all winds on Quesnel Lake and had the energy needed to produce seiche. The 90^{th} percentile used in this study is larger than the 80^{th} percentile used by Thompson but was chosen because it corresponded well to storms that elicited a water response. Events that occurred outside of the 90^{th} percentile wind threshold are not addressed in this thesis.

To search for seiche activity, thermistor data from M14, M9, and M11 was compared to the timing of the isolated storms. Wind forcing ceased once the winds went below the threshold. The resultant displacement of water at M11 was used to estimate the effective height, H_{eff} (**Eq 2-9**). The wave was tracked until the motions became too ambiguous to fit linear wave theory. Seiche period was then predicted using Merian's formula **(Eq. 2-7**) with the East Arm approximated as a 30 km long and 394 m deep rectangular tank. The 30 km extent is the thalweg distance from the tip of the east arm to the reflective shoreline nearest M14, similar to that identified by Brenner (2017). Depth was taken by averaging the thalweg depth over the span of the 30 km extent that seiche was observed. The shallow water approximation was proven valid by $\frac{h_1}{L} < 0.2$, meaning shallow wave theory was applicable to this basin. The system was assumed to have 2 vertical layers and a single horizontal mode, or a V1H1 mode wave isolated within the East Arm. The vertical layer division was placed at the depth of the compensation depth as this was the strongest density gradient in the system.

3.4.4 Temperature trends at 500 m

Unexplained temperature trends had been observed annually in a 10-year time series of data from the 500 m thermistor at M9 (Figure 4.1.2). The data from the 2006-2007 study period was daily averaged to reveal the general trends for that year. A warming trend was defined as the period starting after the deepest surface mixed layer depth of spring turnover and before fall turnover. The winter cooling trend was defined as the period after the first winter storm and through spring turnover. The winter data was divided into three sub-section sections by identifying trends of decreasing or increasing temperature that persisted for longer than 10 days, with a new period beginning on the first day of the change. The bottom temperature time series was compared to a time series of bottom mixed layer growth in relation to the depth of the temperature maximum to describe the trends (Figure 4.4.1). The bottom mixed layer was defined as described in section 3.3.1 and the depth of the temperature maximum was taken from the vertically 1 m interpolated thermistor data.

Chapter 4: Results

4.1 Historical Evidence for Wintertime Deep Water Renewal

Data gathered over multiple field campaigns show evidence of ventilation of deep water in the East Arm of Quesnel Lake. This is seen as increased dissolved oxygen and changes of temperature at 500 m. The temperature data shows recurring trends over winter at the bottom thermistor suggesting annually occurring natural processes are responsible.

4.1.1 CTD Data

Field campaigns during the research period provide several vertical CTD profiles through the east arm at three key periods. Figure 4.1.1 displays casts taken from the M9 and M14 sites, chosen for their depth and location mid length into the East Arm. The first profiles, taken 25 September 2006, align with the end of the summer stratified period, prior to fall weather significantly deepening the surface mixed layer. The next profiles, taken 23 January 2007, are within the beginning of the winter inverse stratification period, specifically during the seiche event initiated by the January Storm, discussed in section 4.3.1. The final CTD profiles were taken 29 May 2007, one month past spring turnover in the early summer stratification period.

CTD casts from September 2006 till May 2007 show a monotonic increase in DO at all depths at both M14 and M9. This indicates that DO was at its lowest after the summer stratified period, was renewed at all depths at fall turnover, and was further renewed during winter inverse stratification and spring turnover. Each set of casts were taken 4 months apart, with an average increase of 0.5 mg/L between summer and early winter, and 1 mg/L between early winter and spring, indicating more oxygen was mixed into the water over winter and in spring turnover than during fall turnover. Its should be noted, that no water samples were taken along with these measurements to test for drift of the DO probe.

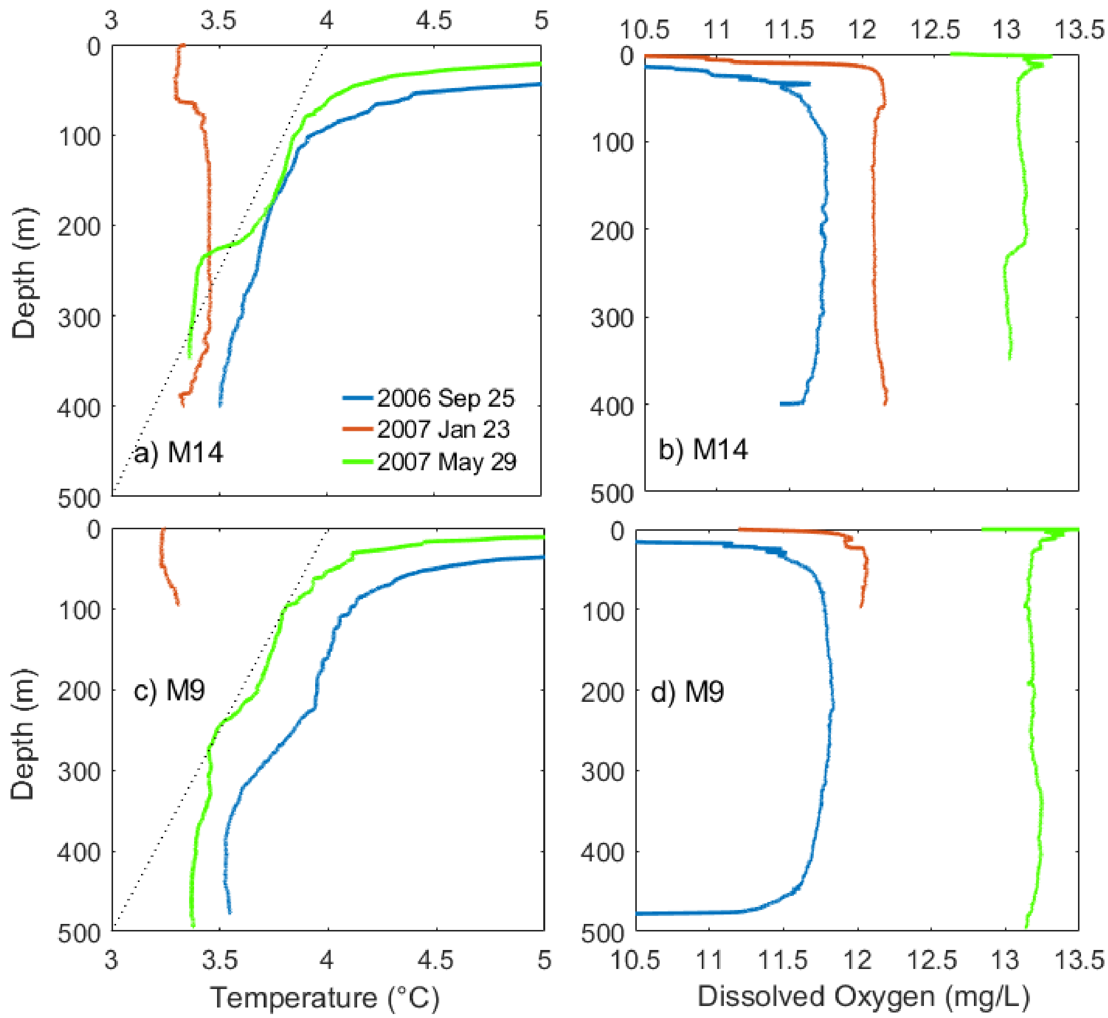

Figure 4.1.1 Temperature (a & c) and dissolved oxygen (b & d) at the M9 and M14 moorings over the study period. Note: Dissolved oxygen was not checked against bottle samples.

4.1.2 Annual Trends

A 10-year temperature time series at M9 500 m depth reveals consistent annual trends of heating and cooling (Figure 4.1.2), with an average annual temperature range of about 0.3°C. Over the 4-month inverse stratification period from late December to mid-April, the water cools. The water then warms over a period of 8 months, from mid-April to late December. The transitions between warming and cooling periods correspond with spring and fall turnovers.

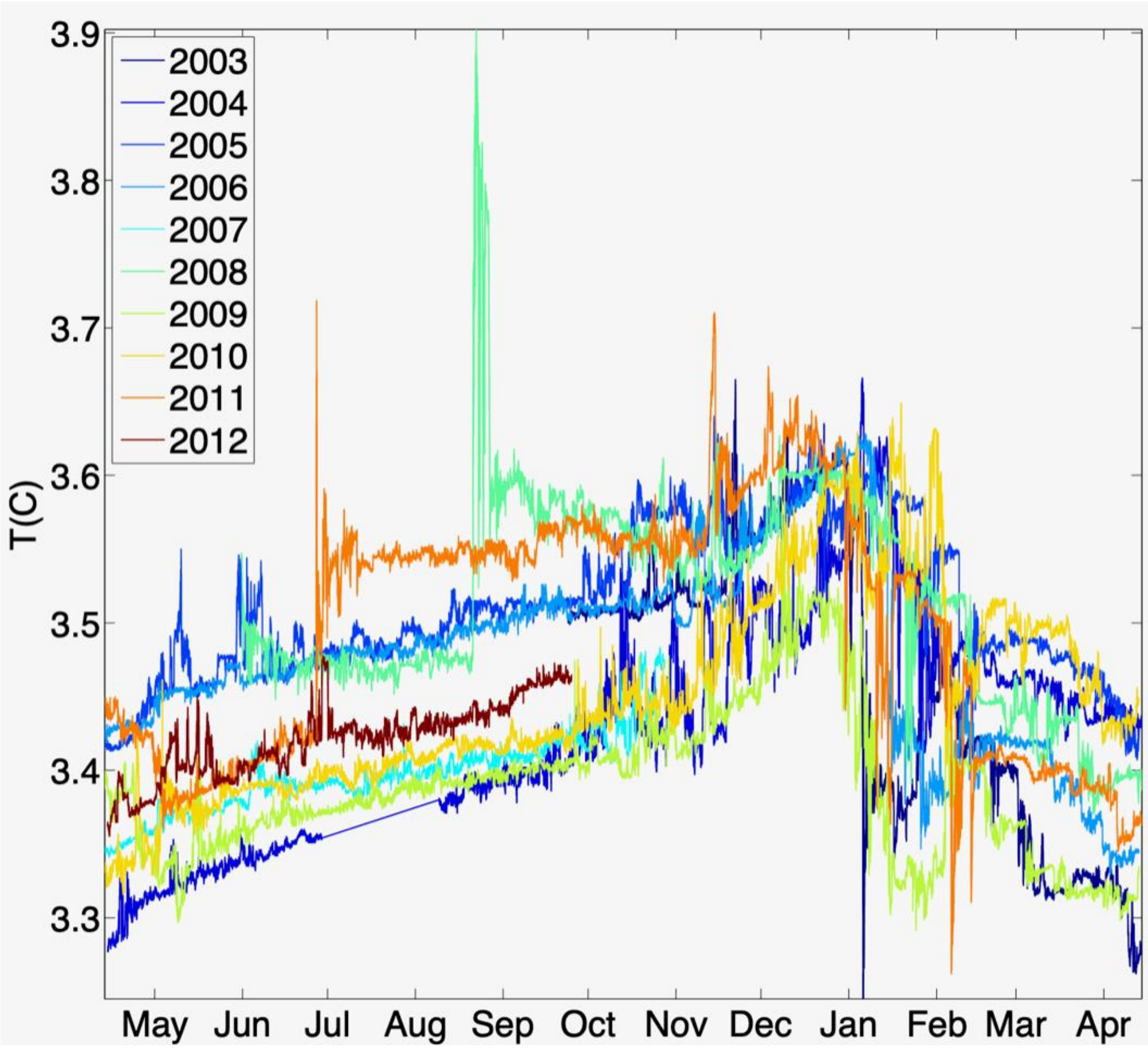

Figure 4.1.2 Temperature record of the 500 m thermistor at M9 between 2003 and 2012. The annual warming and cooling trends are seen in each time series. May – November experiences slow warming, November-January exhibits fast warming, and January-May is cooling with 3 subperiods: fast cooling, warming, slow cooling. (Laval et al., 2014)

The warming period has two distinct subperiods. The minimum temperature at 500 m occurs as spring turnover begins in mid-April each year; the water then slowly warms until the end of the summer stratified period in mid-October. A typical warming of 0.05 - 0.1 °C occurs over this 6-month period. A rapid warming period begins in mid-October to early November of each year and runs until late December, suggestive of increased hypolimnetic mixing likely due to fall storms which are regularly observed in the region. The maximum temperature at

500 m corresponds with the end of fall turnover. The warming over this period is also 0.05-0.1°C, but it occurs more rapidly over roughly 2 months. In 2008 and 2011, spikes of intense warming then cooling can be seen during summer. While these are interesting, they are outside of the scope of this work, which is focused on winter cooling.

The cooling period has three subperiods: rapid cooling, slow warming, and finally slow cooling. In early January of each year, the bottom thermistor experiences rapid cooling of about 0.2 °C over a two- to three-week period. For the 2006-2007 study period, this accounts for 67% of the total cooling at 500 m over the year. Following the rapid cooling each year is a period where the temperature warms slightly or plateaus for about 1 month. The final subperiod shows cooling at about an equal rate as the slow warming period of summer. At the onset of spring turnover, the bottom waters reach their coldest temperature, the summertime slow warming period begins, and the cycle repeats.

The summer warming periods are likely due to vertical diffusive heat exchanges. Slow vertical diffusion of heat through the hypolimnion is a common occurrence in many lakes (Hutter et al., 2011; Imboden & Wuest, 1995). The winter subperiods are not as easy to explain. The January period of rapid temperature drop occurs too quickly to be due to diffusive heat, and as the surface has inversely stratified by this time, it is also unrelated to surface convective mixing. The winter warming period is unexpected as the heat budget indicates that the lake loses heat over the winter. Finally, the change from the warming trend back to a cooling trend, one that is slower than the rapid cooling trend in early winter, has no obvious explanation. Spring turnover has not yet begun at this time, so cold surface water has no mechanism of reaching the bottom. The fact that these trends are present every year suggests that they are not anomalies but rather can be explained by regular physical processes.

4.1.3 Thermistor Data

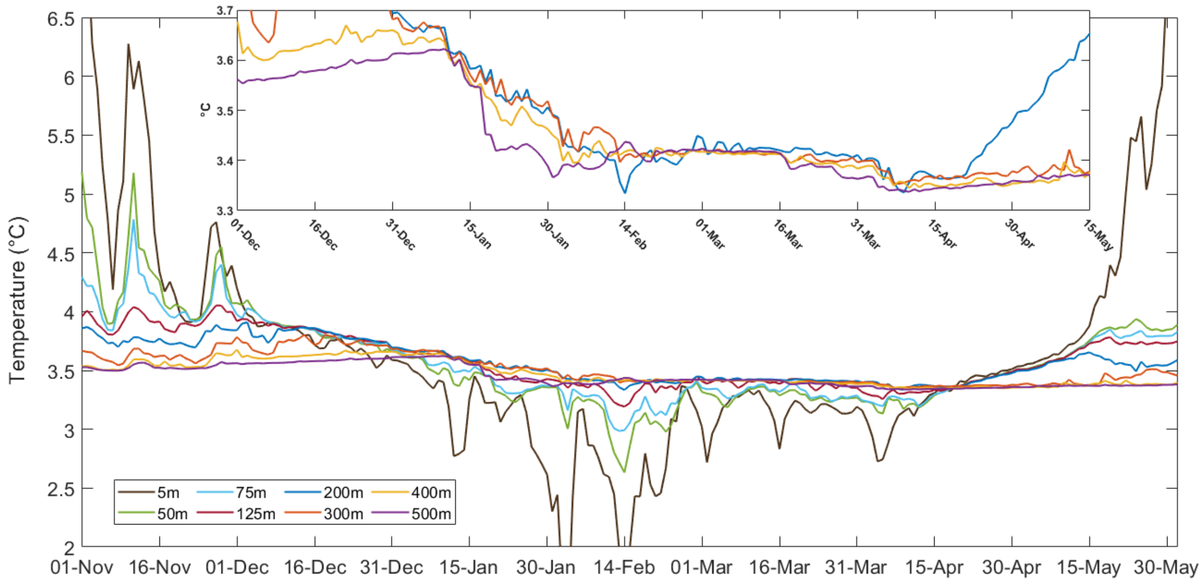

Figure 4.1.3: The fall through early summer progression of the East Arm, with focus on winter inverse stratification. (a) Time series of all thermistors from November 2006 to May 2007. (b) The four hypolimnetic thermistors between December 2006 and May 2007, displaying the three cooling-period sub-periods.

The winter 2006-2007 thermistor record at M9, which is the main focus period of this thesis, is shown in Figure 4.1.3. The 500 m thermistor displays the same cooling and warming trends seen in the ten-year time series shown in Figure 4.1.2. The main panel in Figure 4.1.3 is a time series plot of all M9 thermistors from 1 November 2006 through 1 June 2007. The plot shows typical summertime stratification with large surface fluctuations in early November leading to surface mixing and cooling going into December. In mid-December, many thermistors are homogenous between 50 and 200 m; however, the 5 m thermistor has begun to restratify. Fall turnover is considered to end on 16 December 2006 as this is the final day of positive (stabilizing) buoyancy flux at the surface. Winter inverse stratification becomes clearly visible in the first week of January through mid-April. Spring turnover begins 16 April 16 and entrains all depths for 4 days, after which summer stratification is observed starting 20 April 20.

The subpanel of Figure 4.1.3 focuses on the deep-water thermistors at depths of 200, 300, 400, and 500 m. The deep water at M9 in 2006-2007 begins increasing its rate of warming in early December, aligning with the beginning of fall turnover. The 200 m thermistor becomes entrained into the surface mixed layer during turnover, but the lake surface inversely stratifies before any of the deeper thermistors become homogenized. On 10 January, the bottom four thermistors are all 3.60 °C. This is the maximum temperature recorded at 500 m over the study period and marks the first day of the winter rapid cooling subperiod. On 31 January, the 500 m thermistor has cooled to 3.37 °C, the coldest of all the deep-water thermistors at this time, and the coldest point for the deep water before the warming subperiod of inverse stratification begins. By 14 February the temperature has warmed to a maximum of the subperiod at 3.44 °C. The deep water is homogenized from 26 February to 16 March, with the bottom 4 thermistors homogenous within 0.01°C, and the 300 m to 500 m depths homogenous within 0.007 °C. The deep-water thermistors begin to re-stratify and cool from 16 March to 16 April, the date of spring turnover, when the surface mixed layer reaches the bottom thermistor. The deep-water thermistors are homogenous within 0.03°C until 22 April, when stratification reaches the 200 m thermistor. All bottom thermistors begin to warm beginning the first day of spring turnover.

4.2 Meteorological Results

4.2.1 Heat Budget

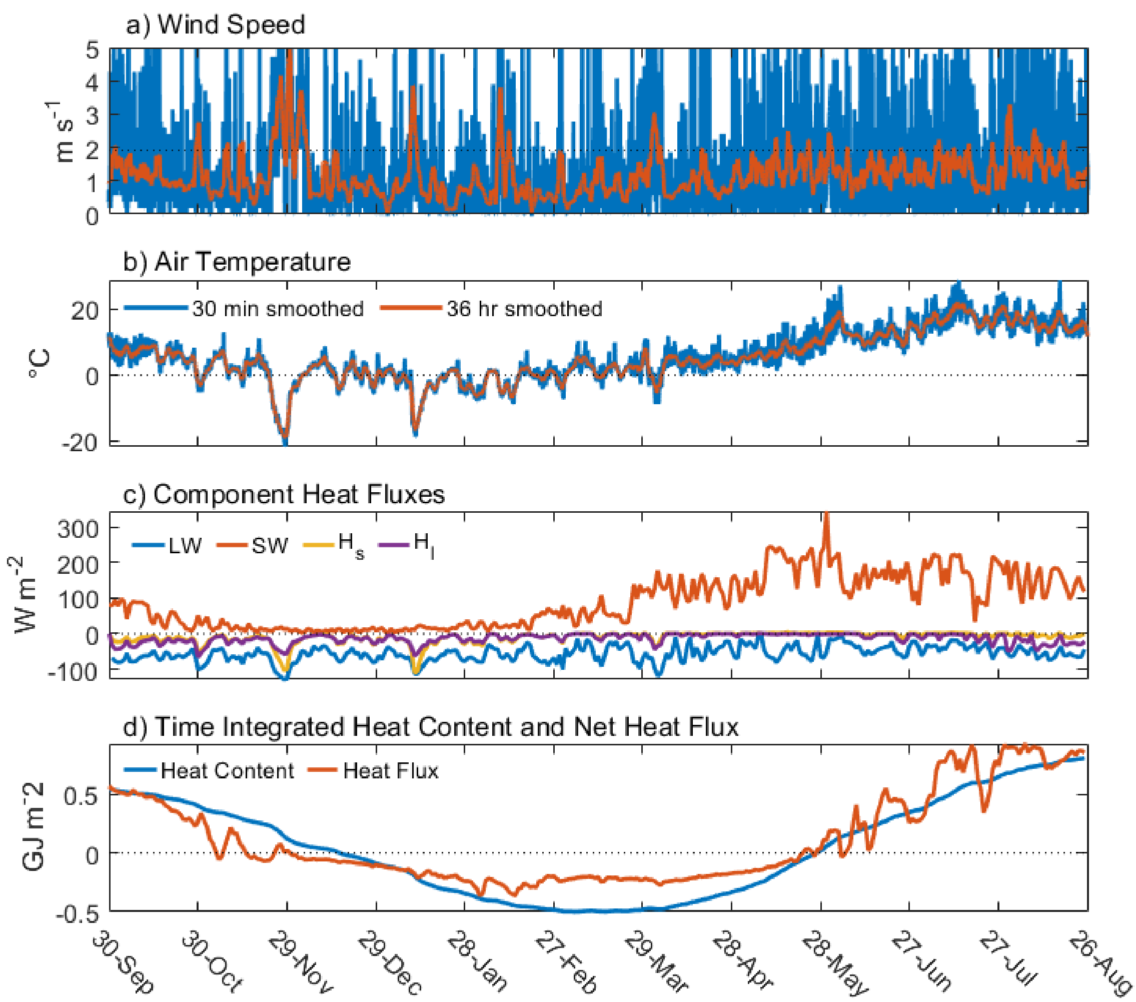

Figure 4.2.1 Meteorological data and resultant heat flux time series from September 2006 – August 2007 from the sources described in section 3.3.2. (a) 30-minute average wind speed (blue) and 36-hr averaged (red) and yearly average (horizontal dashed line). (b) Air temperature 30-minute averaged (blue) and 36-hr averaged (red). (c) Individual heat fluxes, Longwave (LW), Shortwave (SW), Latent Heat (H_l), and Sensible Heat (H_s). (d) Integrated heat content (blue) based on mooring M9 and heat flux (red) of the East Arm.

Figure 4.2.1 is a timeline of meteorological data and heat flux data between September 2006 and August 2007. Panel (a) shows the 30-minute averaged (blue) and 36-hour averaged (red) wind events that occurred between November and early April. The yearly average wind speed was 1.21 ms^{-1}. In fall (27 September 2006 - 05 December 2006), the mean wind speed was 1.39 ms^{-1}, dropping to 0.91 ms^{-1} in the winter stratified period (13 Dec – 16 April), and increasing again to 1.13 ms^{-1} for the summer stratified period (19 April to 25 Aug [end of record]). The yearly average air temperature is 4.95°C. In 2006-2007, the seasonal average air temperature is 0.31 °C in winter, 5.94 °C in autumn, and 12.41 °C for the summer stratified period. The wintertime above-threshold storms had multiple days with temperatures below freezing (Figure 4.2.1b).

Quesnel Lake is at 52° latitude and partly enclosed in mountains. The region experiences mild summers, cold winters, and large wind events throughout the year. Figure 4.2.1c displays a daily-averaged timeseries of the four main component heat fluxes, calculated from meteorological data gathered at the lake side over the period of record. Shortwave radiation is at a maximum of 345 Wm^{-2} over the summer months, a minimum of 1 Wm^{-2} over winter, with an average annual value of 89 Wm^{-2}. Longwave radiation and latent heat are always negative, with average annual values of -56 Wm^{-2} and -14 Wm^{-2} respectively. Sensible heat is mostly negative with an annual average value of -10 Wm^{-2}, though it can become slightly positive (O 1) between spring and fall equinox. The sum of longwave radiation, sensible heat, and latent heat completely negate the incoming energy from shortwave radiation over the winter stratification period. In summer, however, the magnitude of the positive shortwave flux is much greater, and greatly exceeds the outgoing heat flux from sensible heat, latent heat, and longwave radiation. As a result, the annual calculated net heat flux of the lake is 9.3 Wm^{-2} over the 2006-2007 study period.

The heat budget for Quesnel Lake, seen in Figure 4.3.1d, balances well in the East Arm. The net heat flux integrated in time overestimates the heat content of the lake in the fall but predicts the timing of turnover well. The integrated heat fluxes estimate the lake will cross

0 Wm^{-2} several times through November, making the final crossing 30 November 2006. Calculated heat content crosses 0 Wm^{-2}, thus predicting turnover on 16 December 2006. The maximum surface mixed layer depth was found to occur on 13 December. The spring turnover date is estimated very well by the heat fluxes, which become positive on 27 May 2007, the same day as the lake heat content increases above 0 Wm^{-2}, Further, spring turnover as judged by predicted surface mixed layer depth occurred between 16-19 April, a period when temperatures at all depths were homogenous within 0.05°C. It is important to note that the reference temperature for the heat budget was 4°C, whereas the temperature during homogenization was 3.3°C, explaining the discrepancy in timing of spring turnover between the two techniques. In winter (17 December - 27 May), the net heat flux estimate underestimates the net heat content of the lake by 57%. As described in section 4.2.2, this may be attributed to 2-D fluxes within the arm.

Major storms are visible in the individual and net fluxes but are not obvious from the heat content of the lake. The most visible storms are the late November storms that preceded fall turnover and the January storm. Both storms have noticeable rapid decreases in the sensible heat, latent heat, and longwave radiation time series.

4.2.2 Winter Storms

Three major storms were identified during inverse stratification and are highlighted in Figure 4.3.1. The "January Storm" lasts 5 days, from 9-13 January. The "Valentine's Day Storm" was possibly two separate, but consecutive storms occurring between 6 and 12 February. The "Spring Storm" begins 31 March lasting 5 days till 4 April. The series of storms that preceded fall turnover (24 November - 6 December) are also highlighted in Figure 4.3.1 in order to aid in the description of the water column at the onset of inverse stratification.

As outlined in Chapter 3: Methods section 3.4.3, winter storms were isolated via several physical parameters. Identified storms have cold temperatures and higher than average wind speed for prolonged periods blowing from the south (~170°). Wind speed meeting or exceeding the 90th percentile through the year was used to delineate the beginning and end of a storm event. In panels (a) and (b) of Figure 4.2.1, the raw data is shown in blue while the 36-hour averaged data is shown in red. This method, used by Thompson (2019) in his analysis of the wind at Quesnel Lake, is repeated here for consistency and comparability.

4.3 Storm Impact on Water

Figure 4.3.1 presents smoothed meteorological data, analysis of energy at the water surface, and the reaction of the water body over the winter inverse stratification period. Storms are enclosed by dashed lines. Three major storms are discussed: the January Storm, the Valentine's Day Storm, and the Spring Storm. Each storm occurs during one of the winter-time cooling subperiods. The wind speeds depicted in panel (b) reflect the 36-hour averaged wind speeds, highlighted red when the wind reaches the 90th percentile, indicating a significant wind event. Lesser wind events of lesser magnitude occur, but are not fully assessed.

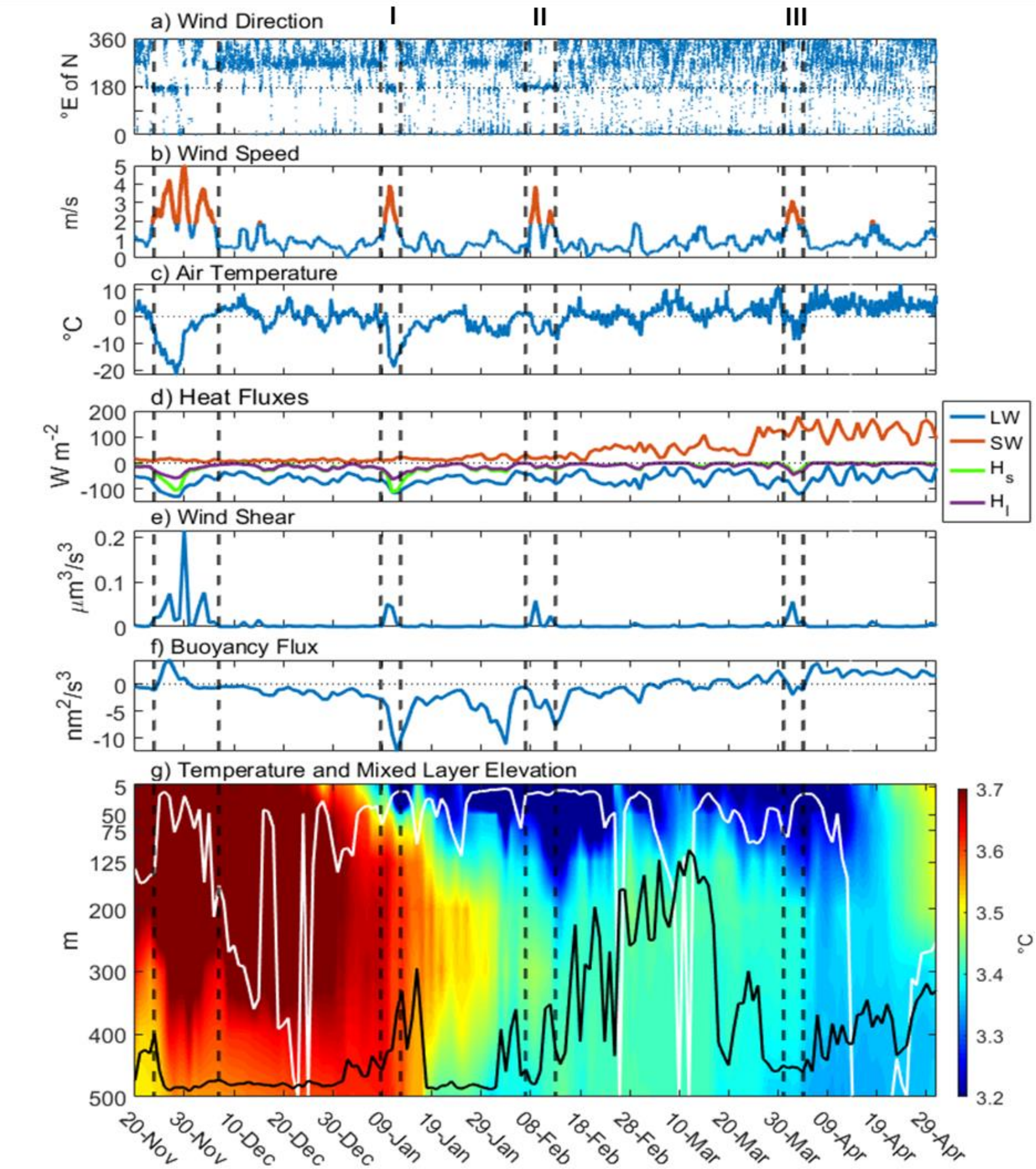

Figure 4.3.1 A time-series of measured data and calculated force s over the study period. The vertical dashed lines indicate I the January Storm, II the Valentine's Day Storm, and III the Spring Storm. (a) Instantaneous wind Direction (b) 36-hour averaged wind speed above (red) and below (blue) the 90th percentile annual speed (c) 30-minute averaged air temperature °C (d) The four component heat fluxes (e) Wind shear at the surface (f) Surface buoyancy flux (g) The interpolated temperature and mixed layer elevation, where the white line is the depth of the surface mixed layer and the black line is the top of the bottom mixed layer.

The water column at the beginning of winter stratification is a product of fall turnover. Fall turnover follows a succession of storms occurring between 23 November and 5 December. During the storms, the surface buoyancy flux at M9 is positive (destabilizing), becoming near zero during turnover as the surface water cools through TMD (Figure 4.3.1f). Wind shear measures as high as 2.15×10^{-7} m^3s^{-3} during the storm and drops to near 0 m^3s^{-3} during turnover. The surface mixed layer reaches a depth of 290 m on 13 December and the temperature range over the full depth of the water column is less than 0.3 °C. By 18 December, surface cooling has restratified the upper waters to 50 m depth indicating the inverse stratification period has begun. It is important to remember that this data set includes the patched wind data as described in section 3.3.2, and the magnitude of the wind speed may be misleading in comparison with other wind data.

4.3.1 January Storm: Rapid Cooling Subperiod

The January storm occurs from 9-13 January 2007, as demarcated in Figure 4.3.1. The storm coincides with the first subperiod of the winter inverse stratification period, the rapid cooling period, and the beginning of the 0.2 °C temperature drop at 500 m in Figure 4.1.3.

The maximum 36-hour average wind speed is 3.7 ms^{-1} (Figure 4.3.1b) and average wind direction (Figure 4.3.1a) is 175°, consistent with a mid-winter mid-latitude low pressure system (Thompson, 2019). The average air temperature (Figure 4.3.1c) is -11 °C, with a high and low of 1.6 °C and -18.8 °C, respectively. Net longwave radiation, sensible heat, and latent heat (Figure 4.3.1d) all decrease over the storm period, hitting a local minimum between 12-13 January with a cumulative value of -290 Wm^{-2}, overpowering the positive shortwave radiation flux of 10 Wm^{-2} and resulting in a net heat loss of -280 Wm^{-2}. Wind shear (Figure 4.3.1e) rapidly grows during the storm to 5.07×10^{-8} m^3s^{-3} on the 10th before returning to pre-storm values by the 13th. The buoyancy flux (Figure 4.3.1f) stabilizes the surface with increasing strength until the end of the high-wind period, at a maximum stabilization value of -12.5x10^{-9} m^{2}s^{-3}. The surface mixed layer of the lake shallows continuously through the storm from 50 m on the 9th to 10 m on the 13th, while the bottom mixed layer thickens from 450 m to 310 m (Figure 4.3.1g).

In the weeks following the high wind event, air temperatures slowly increase but remain below freezing. Surface buoyancy flux weakens with corresponding air temperature increase, lessening the strength of surface stratification. The surface mixed layer deepens and reaches a maximum depth of 90 m on the 25th. The bottom mixed layer does not immediately revert to pre-storm conditions and instead continues to thicken to a max of 290 m on 16 January. By 18 January however, the height of the bottom mixed layer has thinned, reaching only to 480 m and the 500 m thermistor has cooled to 3.45 °C. A thermal maximum exists at 200-300 m during and after the storm, yet the bottom temperature continues to drop to the subperiod minimum of 3.37°C on 31 January.

4.3.1.1 2D Response During the January Storm

The strengthening surface stratification, shrinking surface mixed layer, and thermal maximum at mid-depth over the storm duration indicate that the cooling at depth cannot be attributed to vertical one-dimensional top down convection. A comparison with the M14 and M11 moorings, located on either side of M9, shows that a two-dimensional process is responsible for the cooling of the 500 m thermistor at M9. Large downwelling events occur at M11 and M14 shortly after the storm. Within several days of each downwelling event, cold water appears at depth at M9. The timing and oscillatory nature of the downwelling is indicative of an internal seiche.

To quantify the observed seiche response the span of the East Arm between M14 and M11 was approximated at a 2-D box model as described in section 3.4.3. Though this is a simplification of the actual system, the results hold up well for a full oscillation of the seiche. The East Arm's length and average depth (30 km and 394 m respectively) are significantly greater than the 1 km average width, justifying a 2-D model. Since turnover has only recently occurred, stratification within the lake is still becoming established. The lack of strong stratification means a low number of significant internal waves exist within the lake. The lack of interference from internal waves allow the observed seiche in January to have a linear nature.

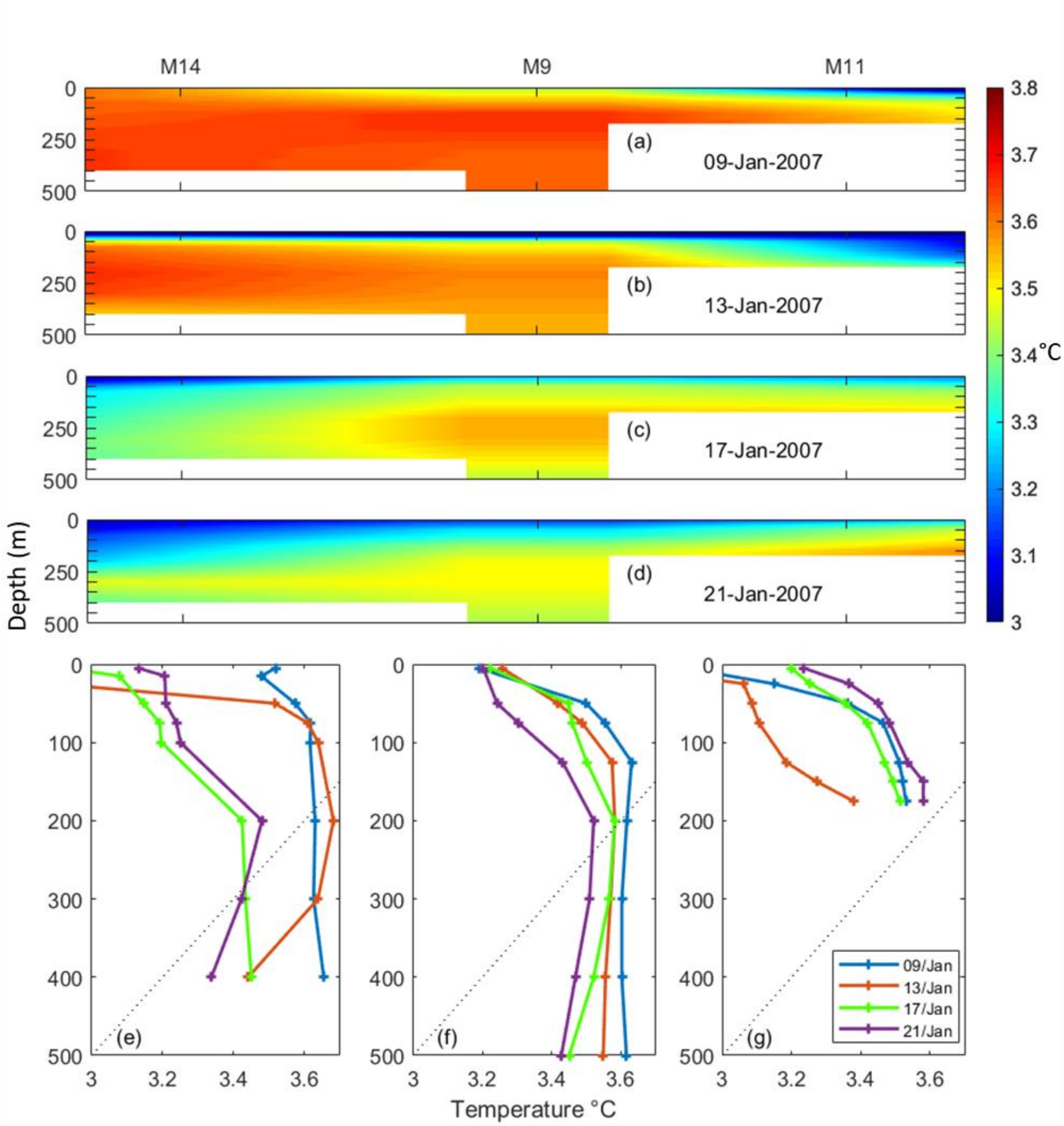

Figure 4.3.2 Spatially interpolated East Arm water temperatures on (a) 9 January 2007 (b) 13 January 2007 (c) 17 January 2007 (d) 21 January 2007, showing the interface deflections created by the January Storm. The daily averaged thermistor record at (e) M14 (f) M9 (g) M11 for the corresponding dates are shown beneath each station, with the diagonal dashed line in each panel representing the TMD profile.

Figure 4.3.2 highlights four dates displaying the downwelling initiated by the January Storm seiche. Merian's formula predicts the period of the baroclinic seiche to be 20 days. This corresponds with the observed downwelling at the antinodes (M14 and M11), which are 8-10 days apart, equal to the half period of the wave. The top 4 panels (a-d) display the horizontally 1 km interpolated daily averaged temperature data along the thalweg of the east arm for each date. The bottom three panels (e-g) show the daily average temperature at each thermistor for each mooring over the same four days.

The wind forcing between 9 and 13 January corresponds with the piling up of cold surface water in the tip of the east arm near M11. Figure 4.3.2 displays the East Arm on the first day of wind forcing, with surface waters beginning to move into the tip of the East Arm. There is a slight deflection of the density interface near M11 and the bottom water at M9 is 3.62 °C. On the final day of the storm, the 13th (Figure 4.3.2b), the surface layer has noticeably cooled over the entire east arm, the bottom water of M9 has cooled to 3.55 °C, and the downwelling at M11 has drastically displaced the density interface to a depth below the bottom thermistor of the M11 mooring. On the 17th (panel c), four days after the wind forcing has ceased, the surface waters have relaxed at M11 and begun to displace the density interface at M14. The bottom waters at M9 have cooled to 3.45°C. Finally, panel d gives a snapshot of the water on the 21st. This panel shows a significant downwelling at M14, the bottom water at M9 has cooled to 4.43°C, and there is an upwelling of warm mid-depth water at M11.

The cooling and warming trends in relation to TMD of each thermistor are displayed in Figure 4.3.2, panels (e-g). The thermistors' depths are marked with an 'x'. The profiles show inverse stratification down to 100-150 m with a temperature maximum that persists between 150 m and 200 m.

The M11 mooring (panel g) records water temperatures of 3.1-3.5 °C below 50 m on 9 January. Cool surface water (<50 m) fully displaces the warm hypolimnetic water by 13 January, when the maximum temperature at the mooring is 3.4 °C at the bottom (175 m) thermistor and the surface is 2.74 °C. The profile from the 17th shows temperatures restored to near the 9 January profile, the first day of wind forcing, at depths below 50 m. The final profile on 22 January shows an increase in temperature at all depths.

Profiles of M14 in panel (e) show the opposite trend to M11. 9 January shows a nearly homogenous profile at M14, with a maximum temperate of 3.65 °C at 400 m and a minimum of 3.48 °C at 15 m. On the 13th, depths between 100 m and 300 m at M14 have warmed, while the surface has cooled to 2.12 °C, and the 400 m water has cooled 0.2° to 3.45 °C. Note that the warmest temperature at M14 is at 200 m on 13 January while the coldest point at M11 is at 175 m on same date. The profile on the 17th shows drastic cooling at all depths but 400 m, in contrast to the warmed profile at M11. The 200 m thermistor has crossed TMD and the 300 m thermistor is on the TMD line. Finally, on the 21st, there is warming at all depths above 300 m, while the 400 m thermistor has cooled further to 3.34 °C.

The M9 thermistor chain is located at a node between M11 and M14 and shows continuous cooling at all depths. The 500 m thermistor cools continuously from 3.62 °C to 3.55°C, 3.45°C, and finally 3.43 °C over the four dates displayed. The 200 m thermistor is very close to TMD on the 9th, crosses but remains close to TMD on the 13th and 17th, then finally cools below TMD by the 21st. Over the entire period the surface thermistor shows little fluctuation, varying in temperature between 3.19-3.26 °C.

The dates of the largest observed cooling events of the 500 m thermistor occur on 17 January and 26 January. These correspond to 4 and 5 days respectively after the observed downwellings. This would indicate a bottom water flow velocity from M11 and M14 to M9 at roughly 2.6 cm s^{-1}.

4.3.2 Valentine's Day Storm: Warming Subperiod

The second subperiod of winter stratification, the warming period (Figure 4.1.2), begins 31 January. Between 31 January and 20 February, the 500 m thermistor warms from 3.36 to 3.42 °C (with a max temperature of 3.43 °C on 14 February). From 21 February to 16 March, the temperature plateaus at 3.42 °C and does not vary more than 0.005 °C. There is one large storm, the Valentine's Day Storm, and two short wind events during this subperiod. The Valentine's Day Storm begins 8 February and lasts 5 days. The two small wind events occur 28 February and 14 March and last ~1 day each.

The evolution of surface stratification and the complex geometry of the lake make internal wave motion too complicated to be linked directly to wind forcing using linear theory. We therefore take the assumption evidenced by the January storm that the reaction of the 500 m thermistor is related to seiche-driven downwellings which occur after storms. There are observed thermobaric downwellings between 12-14 February at M11 and on 11 March at M14.

The Valentine's Day Storm occurs from 8-12 February 2007 (Figure 4.3.1). The 36-hour averaged wind speed has a maximum value of 3.8 (Figure 4.3.1b), and wind direction (Figure 4.3.1a) is 175°. The average air temperature (Figure 4.3.1c) is -3.8 °C, with a high and low of 0.7 °C and -6.8 °C, respectively. All fluxes stay relatively constant through the storm with a net heat loss of -13.05 Wm^{-2}. Wind shear (Figure 4.3.1e) peaks in concert with wind speed, with peaks of $5.8x10^{-8}$ m^3s^{-3} on 9 February and $2.3x10^{-8}$ m^3s^{-3} on 11 February. Much like the January Strom, buoyancy flux (Figure 4.3.1f) decreases through the entire storm, stabilizing the surface, with a value of $-0.6x10^{-9}$ m^2s^{-3} the first day of the storm to a peak of -7.7×10^{-9} m^2s^{-3} on the final day of the storm. The surface mixed layer remains largely unchanged before, during and after the storm, ranging between 5-20 m depth. The bottom mixed layer (Figure 4.3.1g) begins its largest growth period beginning with the Valentine's Day Storm. The bottom mixed layer thickness ranges between a minimum at 480 m on 9 February and a maximum at 100 m on 12 March.

The temperature of the M9 500 m thermistor rises through the Valentine's Day Storm and reaches a local maximum of 3.44 °C on 14 February then begins to cool to 3.40 °C on the 19th. The local cooling at 500 m occurs 5 days after the downwelling event at M11 on the 14th. This is similar to the lag before cool water from M11 reached M9 following the January Storm.

The two small wind events (28 February and 14 March) exhibit the same properties as the January and Valentine's Day storm, but to a lesser degree. The storms have 36-hour averaged winds peaking at 2 ms^{-1} and decreased air temperatures dipping below freezing. Both see a slight increase in wind shear and stronger stabilization from the buoyancy force. The surface mixed layer contracts during both wind events while the bottom mixed layer continues the growth that began 9 February. The thermobaric instability seen at M14 on 11 March occurs 5 days before the peak cooling at M9 on 16 March, marking the end of the second winter subperiod.

4.3.2.1 2D Response During Valentine's Day Storm

Figure 4.3.3 displays the 2D response of the lake on key dates during and following the Valentine's Day Storm. Panels (a)-(d) show the horizontal interpolated temperature contour from M14 to M11, while (e)-(f) show the thermistor profiles at each location for the corresponding dates. The Valentine's Day Storm is much less linear than the January Storm and experiences interaction from other internal waves. Therefore, a seiche period is not estimated, instead the thermobaric instabilities created by wind induced downwelling is described.

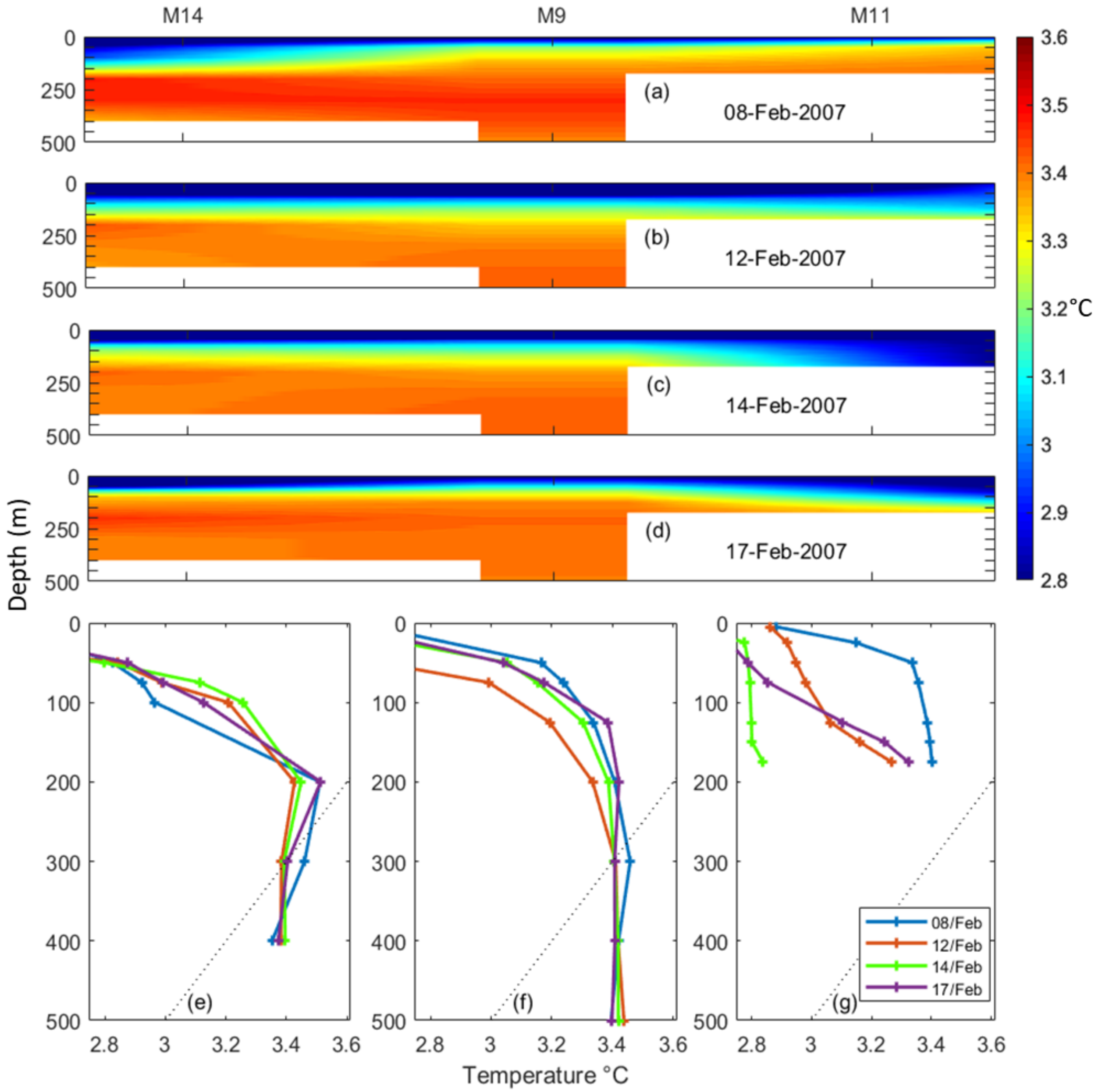

Figure 4.3.3 Spatially interpolated East Arm water temperatures on (a) 8 February 2007 (b) 12 February 2007 (c) 14 February 2007 (d) 17 February 2007, showing the interface deflections created by the Valentine's Day Storm. The daily averaged thermistor record at (e) M14 (f) M9 (g) M11 for the corresponding dates are shown beneath each station, with the diagonal dashed line in each panel representing the TMD profile.

The first and final days of the Valentine's Day Storm are shown in panels (a) and (b), respectively. Previous wave motions have created an interfacial set down toward M14 on 8 February (panel (a)). There is an obvious temperature maximum of about 3.46 °C at the compensation depth and the 500 m thermistor at M9 registers at 3.39 °C. On 12° February (panel (b)), the final day of the storm, the interface tilt has shifted and is beginning to set down toward M11. The temperature maximum at M9 has warmed to 3.44 °C and but has been displaced downward to 500 m becoming buoyant relative to the water at 400 m, creating an unstable water column. Panels (e) and (f) show water crossing TMD between 200-300 m from the 8th to the 12th at M14 and M9, respectively. This indicates that several thermobaric instabilities were triggered at the compensation depth during interfacial tilts over the Valentine's Day Storm.

By 14 February, the interfacial shift has reached its greatest tilt toward M11 (panel (c)). The M9 thermistors at 300, 400, and 500 m have homogenized to 3.42 °C (panel (f)). Panel (g) shows the water temperature at M11 on the 12th registers at 3.27 °C, equivalent to TMD(z) between 300-400 m depth. On the 14th, all the water at M11 is below 2.8°C, colder than TMD(z) for any depth in the lake. This indicates the thermobaric instability was likely triggered in between M11 and M9 during the interfacial shift. This event coupled with the events at M9 and M14 from the 8-12th could have provided sufficient mixing to have homogenized the bottom 300 m of the water column.

On 17 February (panel (d)) the density interface is beginning to restore to neutral from its set down at M11. At this time, the temperature maximum has diminished in thickness and temperature, and the bottom water between 200-500 m is homogenous within 0.03 °C.

The bottom mixed layer begins its largest growth period following the Valentine's Day Storm (Figure 4.3.1). On the first day of the storm, 8 February, the bottom mixed layer thickness is 480 m. On 12 February, there is a local peak of 330 m in bottom mixed layer thickness. This timing is consistent with thermobaric instabilities occurring at M9 between the 8-12 February. On the 17th, the bottom mixed layer thickness has reached 230 m. This is 5 days after the thermobaric instability occurred between M9 and M11 from 12-14 February. As evidenced by the January Storm, the required time for water from set downs at M11 to reach M9 is approximately 5 days. This is repeated by the Valentine's Day. Water set down near M11 on the 12th arrived at M9 on the 17th.

4.3.3 Spring Storm: Slow Cooling Subperiod

The last of the three winter subperiods is the slow cooling subperiod. This subperiod begins on 16 March and continues until 10 April. The bottom mixed layer has thinned from its maximum thickness reaching to 160 m below surface on 16 March, to a minimum thickness reaching only 450 m below the surface on 6 April. The 500 m thermistor records a bottom temperature of 3.41°C on 16 March, cooling by 10 April to 3.34°C, the annual minimum for 2007. This is 0.28 °C colder than the annual maximum of 3.62 °C recorded on 10 January.

In the slow cooling subperiod, there is one large storm event. The Spring Storm occurs from 31 March to 4 April (Figure 4.3.1). The maximum 36-hour averaged wind speed is 3.0 ms^{-1} (Figure 4.3.1b), and the wind direction (Figure 4.3.1a) is 175°. The average air temperature (Figure 4.3.1c) is 2.4 °C, with a high and low of 2.3 °C and -8.9 °C, respectively. By now shortwave radiation, averaging 89.1 Wm^{-2}, dominates the other fluxes which are all negative. Although shortwave radiation is attenuated during the storm, the average net heat flux is 9.8 Wm^{-2}. Wind shear (Figure 4.3.1e) peaks at 5.6 $x10^{-8}$ m^3s^{-3} on 2 April. Buoyancy flux is positive (stabilizing) immediately before and after the storm. During the storm, buoyancy flux fluctuates between negative and positive values, averaging $1.3x10^{-9}$ m^2s^{-3}. The bottom mixed layer (Figure 4.3.1g) thins from 440 m to 450 m below the surface during the storm but grows immediately after the storm with a maximum thickness reaching 320 m below the surface on 9 April. Growth continues through spring turnover on 16-19 April and into the summer stratification period. The surface mixed layer shrinks from 30 m to 10 m over the storm period but grows immediately after the storm to 500 m depth for spring turnover. There is an observed downwelling event at M14 on 27 March, which corresponds with cooling at M9 on 1-2 April (Figure 4.3.4).

A key difference between the Spring Storm and the other major winter storms is that by this time, buoyancy flux has become positive (destabilizing) and the surface mixed layer grows substantially post-storm, leading to spring turnover. The water column is homogenous at 3.34 °C. This marks the end of the slow cooling period and winter inverse stratification. The surface is stratified, and the bottom begins to warm slowly due to down gradient diffusion.

4.3.3.1 2D Response During the Spring Storm

Figure 4.3.4 displays the 2D response of the lake on key dates prior to, during, and following the Spring Storm. Panels (a) and (b) show the horizontal interpolated temperature contour from M14 to M11 prior to the Spring Storm. Panels (c) and (d) display the first and last days of the 5-day storm. Panel (e) shows the temperature contour 2-days post storm, 10 days prior to spring turnover. Panel (f)-(h) show the corresponding thermistor profile for those dates.

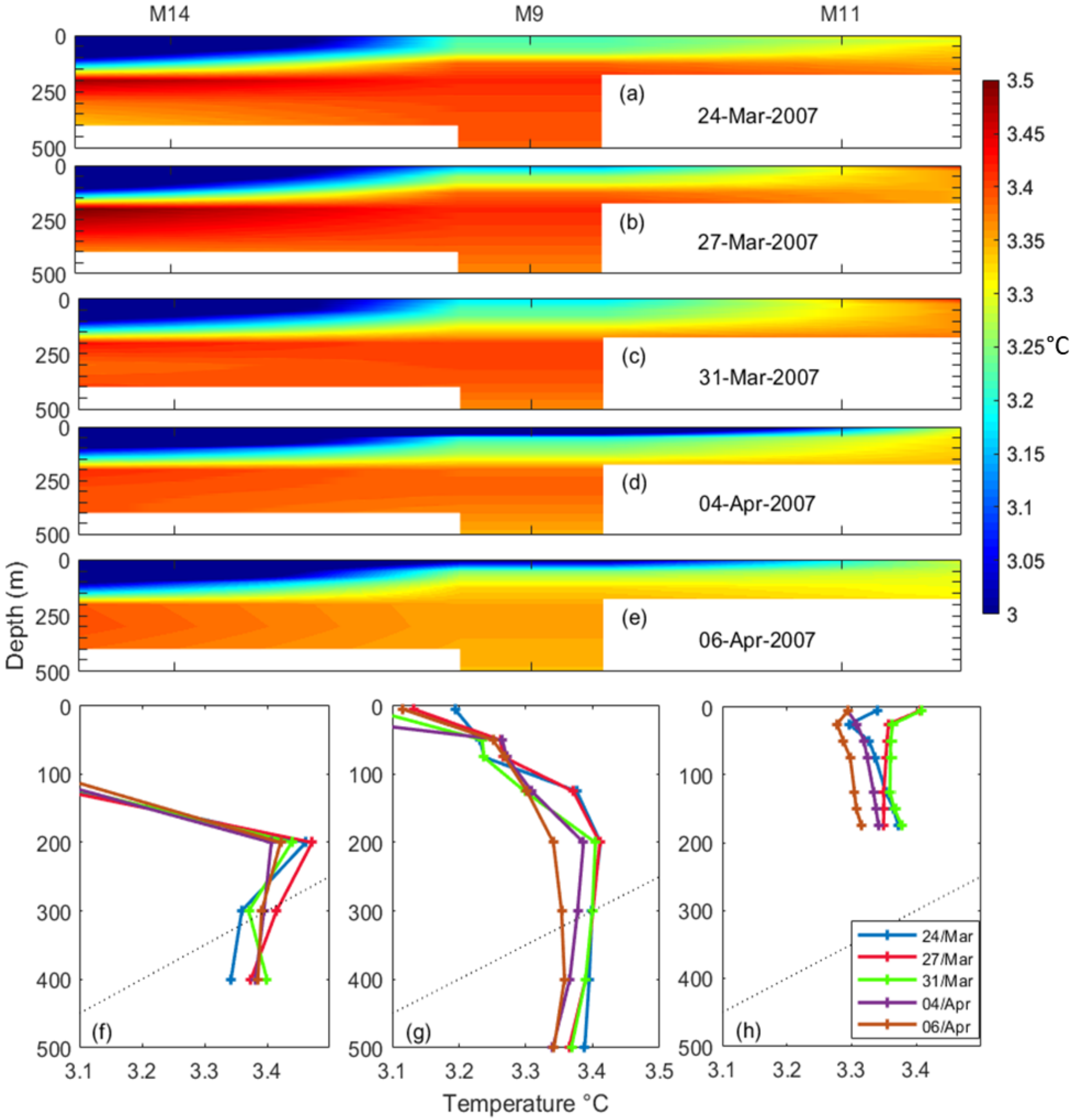

Figure 4.3.4 Spatially interpolated East Arm water temperatures (a) 24 March 2007 (b) 27 March 2007 (c) 31 March 2007 (d) 4 April 2007 (e) 6 April 2007, showing the interface deflections created by the Valentine's Day Storm. The daily averaged thermistor record at (f) M14 (g) M14 (h) M11 for the corresponding dates are shown beneath each station, with the diagonal dashed line in each panel representing the TMD profile.

The Spring Storm (31-March to 4-April) assists in the break down of the thermal maximum by creating mixing both above and below the compensation depth, homogenizing the water column at M9. This occurs from a combination of large upwelling events at M11 and thermobaric instabilities at M14 and M9. A strong tilt of the density interface near 100 m depth is present between M14 to M11 through the entire 13-day period shown in Figure 4.3.4 (panels (a)-(e)). This creates a horizontal temperature gradient along the East Arm. Set down at M14 causes upwelling at M11 and thermobaric instability at M14. M14 experiences continuous warming and homogenization of deep water below 200 m (panel (f)), whereas M11 homogenizes and cools over the period (panel (h)). Between 24 March to 6 April the ΔT between the thermal maximum and 500 m at M9 change from 0.032 °C to 0.016 °C.

From 31 March to 4 April, the 500 m thermistor at M9 cools 0.016 °C (panel (g)). The 300 m thermistor at M14 (panel (f)) crosses through TMD between 24-27 and 27-31 March, triggering thermobaric instabilities. This corresponds with 4-6 days of transport time between M14 and M9. Over this same time interval (24-31 March) the 300 m thermistor at M9 is at its compensation depth. Between 31 March and 4 April (the first and last day of the Spring Storm), the 300 m thermistor crosses TMD triggering a local instability, aiding to cooling at 500 m. The first day of the Spring Storm the bottom mixed layer thickness does not exceed 460 m (Figure 4.3.1). The bottom mixed layer grows to a maximum thickness of 370 m on 7 April, but then contracts to 410 m by 16 April, the first day of spring turnover.

Panel (h) shows continuous convective mixing and a general cooling trend of the entire water column at M11 due to the continuous upwelling. This cooling trend is reflected in the M9 200-300 m thermistors which cool similarity over the same time frame. Panel (g) shows the M9 mooring cools significantly from 200 m downward to 500 m between the 31-March and 6-April. The 200 m thermistor cools by 0.07° C, the 500 m thermistor cools 0.04° C, and the thermal maximum changes from 3.4° at 200 m to 3.36° at 400 m.

4.4 Impact of the Interaction of the Bottom Mixed Layer and the Thermal Maximum

In the previous sections, cooling events at 500m depth are linked to thermobaric instabilities triggered by wind-driven downwelling. Observations indicate water downwelled near M14 and M11 will arrive at M9 within 5 days, explaining discrete cooling events over short time scales. This does not, however, explain the annually observed longer term trends lasting on the order of weeks to months. Here is a proposed mechanism to explain this phenomenon.

The warming or cooling at 500 m is dependent on the bottom mixed layer and its position in relation to the depth of subsurface temperature maximum, which occurs at or near the compensation depth. The thickening of the bottom mixed layer follows large storm events. As the bottom mixed layer thickness expands upwards towards the depth of the thermal maximum, it entrains overlying warmer water thereby warming the bottom mixed layer. If the bottom mixed layer continues to expand above the depth of the temperature maximum, cooler near-surface water is entrained, thereby cooling the bottom mixed layer.

Figure 4.4.1 highlights three subperiods of winter determined by the general trend of temperature measured at 500 m (panel a). The first subperiod of winter, the fast cooling subperiod, encompasses the January storm. The growth of the bottom mixed layer from the January storm is relatively small and short-lived and this period is dominated by two large pulses of cold water due to thermobaric instability (Figure 4.3.1). During this subperiod, the upper limit of the bottom mixed layer remains more than 100 m below the thermal maximum depth.

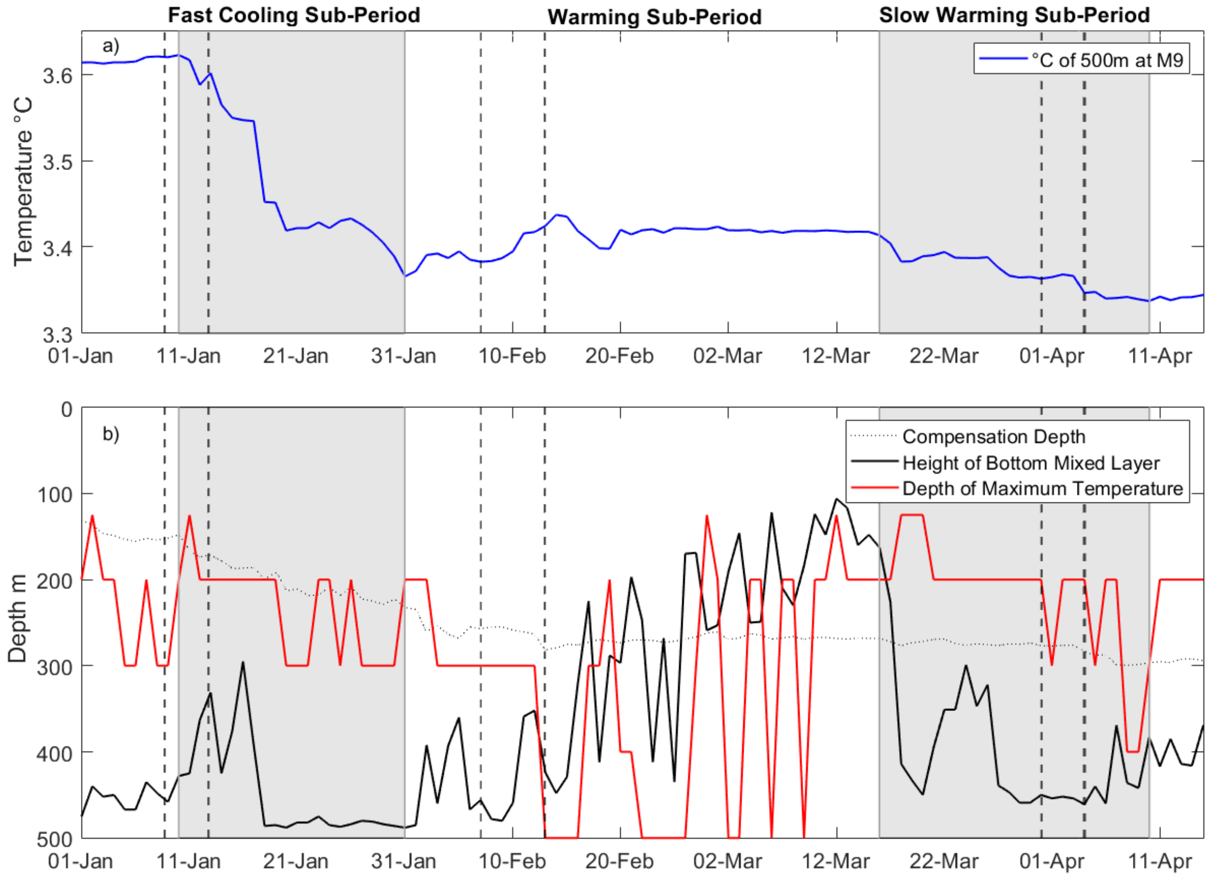

Figure 4.4.1 The temperature record at M9 500 m over the study period (panel a) and the interaction between the bottom mixed layer and temperature maximum (panel b). Vertical dashed lines delineate the three storm periods discussed in 4.2.2. and the alternating shading regions delineate the periods of warming and cooling seen at M9 500 m as labeled at the top of panel (a).

The second subperiod of winter, the warming subperiod, encompasses the Valentine's day storm. This period is characterized by an abundance of internal waves leading to increased near-bottom mixing and only one large observed thermobaric instability (Figure 4.3.3). During this subperiod, the bottom mixed layer continuously expands, and reaches its maximum observed thickness, estimated at 100 m below the surface. As the bottom mixed layer extends upwards toward the temperature maximum, it entrains warmer water thereby warming this homogenized layer. Thereafter the bottom mixed layer stops growing, creating a plateau in temperature at 500 m. Note that as the bottom mixed layer reaches the compensation depth, the position of the temperature maximum becomes erratic, with large jumps from thermistor to thermistor. The threshold for identifying the bottom mixed layer is 0.02 °C, and so the erratic behavior is misleading, as the temperature of the entire layer is near homogenous, thus temperature maximum has a more ambiguous location.

The third and final subperiod of winter, the slow cooling period, begins 5 days after the 11 March 2007 thermobaric instability at M14. The bottom mixed layer retracts rapidly, with its upper limit reaching to only 440 m below the surface, while the depth of the temperature maximum remains near the compensation depth at 200 m. The Spring Storm occurs between 31 March and 4 April 2007, initiating thickening of the bottom mixed layer. By this time surface buoyancy flux is positive (destabilizing), and the surface mixed layer is deepening. The 500 m thermistor stops cooling on 10 April 2007. By 16 April the surface mixed layer has reached the 500 m thermistor, marking full spring turnover has occurred.

These processes link the annual temperature trends seen in Figure 4.1.2 to the seiche events observed over the 2006-2007 winter (Figures 4.3.2, 4.3.3, 4.3.4). The implications of this are that the deep waters of the East Arm experience regular ventilation each winter due to the processes described in this chapter.

Chapter 5: Discussion

5.1 Implications for Deep Water Renewal

Decades of research on thermobarically stratified lakes such as Lake Baikal, Crater Lake, and Norwegian lakes (Hornindalsvatn, Mjøsa Tinnsjø, Tyrifjord, and Breimsvatn) among others have revealed several instances of deep water renewal by thermobaric instability. Thus, ventilation by thermobaric instability in Quesnel Lake is not a surprising result. Indeed, this study adds support to an extensive volume of evidence. However, the prevalence and annual regularity of seiche motion under inverse stratification, and the successfulness of spring turnover in Quesnel Lake is more unique. While other deep lakes have demonstrated these same processes, many have not, and fewer still have evidence of such regular trends. The subtle characteristics that lead to a well or poorly ventilated deep lake are worth further consideration.

Boehrer et al. (2013) conducted a study of five deep, thermobarically stratified fjord-type lakes in Norway that have many similarities to Quesnel Lake. All the lakes were well ventilated, and spring turnover was found to be more effective than fall turnover. Further, spring turnover was found to reset the bottom temperature for the annual cycle. This was the same result found in Quesnel Lake, where the annual temperature minimum was reached at the end of the slow cooling sub-period, just before spring turnover. Spring turnover marked the beginning of the annual summer warming period, as observed in Figure 4.1.2. The study by Boehrer et al. utilized data from the year 2006 only and made no reference to the regularity of the ventilation of bottom water. However, as the paper itself states, longer lakes have more potential for longitudinal gradients leading to thermobaric instability. This suggests that ventilation in the lakes in the Boehrer et al. study is likely because, like Quesnel Lake, their geometry allows for wind setup to effectively displace surface waters to a point of negative buoyancy.

Crater Lake, at 589 m depth and ~8 km in diameter, is also prone to thermobaric instability but does not experience full turnover (Crawford & Collier, 1997). The most significant difference between Quesnel Lake and Crater Lake is geometry, where Crater Lake (as the name implies) is a round caldera lake. The results of a 14-year study found Crater Lake's hypolimnion showed smoothing of temperature and salinity gradients by thermobaric plumes, but the rate of ventilation varied year to year. The study showed thermobaric instabilities would only occur if the epilimnion had weak stratification and extended to the mid-depth layer at or near the compensation depth (200-300 m). This is the inverse of what is observed at Quesnel Lake, where the strength and relative layer shallowness of the stratification is what allows wind setup to be so successful in inducing thermobaric instability, as energy is not dissipated through surface mixing. The thermobaric instabilities in Crater Lake occur less often and do not persist through the inverse stratification period as they do in Quesnel Lake. The instabilities are still storm-induced; however, Crawford & Collier (2007) found that Crater Lake has no natural mode of oscillation. This means that unlike Quesnel Lake where ongoing seiche oscillation is observed, seiche cannot be set up in Crater Lake.

Lake Baikal is the deepest lake in the world and has a significant body of research focused on its thermobaricity. Unlike Quesnel Lake and the Norwegian lakes, Carmack & Weiss (1991) predicted a more successful fall turnover than spring turnover in Lake Baikal. Lake Baikal's surface is covered by thick ice in spring, damping the wind forcing. As the authors state, a thermobaric instability in spring is less likely than in fall, simply due to the lack of mechanical forcing provided by storm activity. In contrast, at Quesnel Lake, the lack of ice cover in the East Arm over winter and spring turnover allows for direct momentum transfer from winter storms to the water.

One of many differences between Quesnel Lake and Lake Baikal is depth. Baikal's extreme depth (1632 m) allows for thermobaric instability and a well-ventilated bottom layer, while at the same time having older water within a much thicker mid-depth layer. The research presented in this thesis has shown the bottom mixed layer in Quesnel Lake is extremely important to a successful spring turnover. It is possible that Lake Baikal's geometry does not allow for a bottom mixed layer to grow to a height where it can interact with the mid-depth layer, meaning the mid-depth layer acts as a barrier to seasonal turnover. Like Quesnel Lake, the surface layer in Lake Baikal is roughly 200-300 m in depth, representing the depth to which convection alone can mix the water column. This corresponds with the compensation depth, where $\alpha = 0$ and buoyancy flux changes sign. In Quesnel Lake, the dual action of both the surface and bottom mixed layers growing toward and eroding the middle depth layer is what allows for a full spring turnover. In Lake Baikal, the mid-depth layer is simply too large to be overtaken by this same mechanism, thus contributing to a fall turnover that is more successful than spring.

5.2 Implications in Combination with Previous Research on Quesnel Lake

Earlier research by Laval et al. (2008), Brenner (2017), and Thompson (2019) provide significant evidence that wind forcing is a major mechanism of mixing and transport in Quesnel Lake. The results of this study support these earlier conclusions, showing that both vertical and horizontal transport is catalyzed through baroclinic seiche events within the East Arm of Quesnel Lake.

Laval et al. (2008) identified a seiche-induced exchange flow located at the Cariboo Island Sill dividing the West Basin from the main body of Quesnel Lake. The seiche events were observed during summer stratification, exchanged mainly hypolimnetic water, and the fundamental seiche period of the lake was found to be ~6 days. Research by Thompson (2019) identified storm types with sufficient energy to initiate the seiche described by Laval et al. This study utilized Thompson's methods to show that the three storms identified and described in Section 4.2.2 fit the description for seiche-inducing storms.

Brenner (2017) utilized Merian's equation to model barotropic seiche throughout Quesnel Lake. A node identified in Brenner's research corresponded with the M9 mooring location in this study. M9 was identified as the major node of the East Arm winter seiche events, with anti-nodes identified at M11 and M14. All storms produced isotherm displacements at M11 and M14. The January Storm event followed linear wave theory and had a second vertical mode seiche period matching the period predicted by Merian's equation.

Research by Hamilton et al. (2020) analyzed turbidity in the West Basin following the Mt Polley Mine disaster. Hamilton acknowledges the presence of a benthic boundary layer containing continuously suspended turbid material in the West Basin following the spill. This layer was considered a main source for resuspended sediment in the years following the initial spill. Hamilton et al. analyzed pre- and post-spill data and theorized that the elevated levels of turbidity post-spill were the result of tailings sediment having been resuspended via shearing from baroclinic seiche. Similarly, the bottom mixed layer in the East Arm was shown to grow after storm events initiated seiching, inducing shearing and turbulent mixing.

Granger's research assessed sources and sinks for the suspended sediment in the West Basin over the first four years post spill. The main body of the lake is identified as a continued source of spill-associated sediment into the West Basin. Granger's results suggest that ~80% of the suspended sediment flowed into the main basin of Quesnel Lake by 2014 September. The tailings plume reached the main body of the lake within weeks of the spill, and was measured as far as the junction at M8 before measurements stopped for winter (Petticrew et al. 2015). Hamilton et al. presents evidence from turbidity sensors that the plume extended further, to M14, by late November 2014.

5.3 Implications for Future Research

Possible sources of error of this study include data gaps in measured field data and assumptions made through interpolations and simplifications. The assumption that salinity is homogenous and constant throughout the lake neglects to account for the impact of salinity gradients in stabilizing the water column. The East Arm was interpolated horizontally using only three moorings, leading to poor horizontal resolution. To predict the seiche period the east arm was simplified to a 2D box model with only two vertical modes. Only the January Storm could be used to clearly predict seiche periods as wave motion in the East Arm quickly become non-linear. Wave interaction from elsewhere in the lake was ignored. Further, horizontal gradients and differential cooling were ignored. With further data collection and research many of these topics could be investigated or resolved.

Chapter 6: Conclusion

The results presented in this study have shown that the deepest waters of Quesnel Lake are substantially renewed over winter and during spring turnover, primarily from thermobaric instabilities and from entrainment due to surface and bottom mixed layer growth. The thermobaric instabilities occur during wind-induced baroclinic seiche events created by large winter storms. These seiche events generate shear at density interfaces and at the lakebed. Shear-induced turbulence homogenizes the bottom water of the lake, growing the bottom mixed layer. The convergence of the bottom mixed layer and the surface mixed layer lead to a full turnover in spring, homogenizing all 500 m of the water column to within 0.05 ºC. Spring turnover resets the bottom temperature and restarts the lake’s annual temperature cycle.

This study connected the observations of annual temperature trends in the deepest waters of Quesnel Lake with its bottom mixed layer. The position of the bottom mixed layer in relation to the meso-temperature maximum dictates the temperature of the water at 500 m during the inverse stratification period. Growth of the layer toward the temperature maximum entrains warmer water, increasing the temperature at 500 m. Growth above the temperature maximum entrains colder water, cooling the temperature at 500 m.

Bibliography

A. Bronsro, Ogilvie, J., Adams, M., & Nikl, L. (2016). River rehabilitation following a dam breach, 190–201.

B. Laval; S. Vagle; J. Morrison; Carmack, E. (2014). Deep water ventilation of a fjord lake: 10 years of observation from Quesnel Lake, Canada. Trento, Italy.

BC Geographical Names Office. (2020). Lakes. Retrieved July 10, 2020, from https://apps.gov.bc.ca/pub/bcgnws/

Boehrer, B., Fukuyama, R., & Chikita, K. (2008). Stratification of very deep, thermally stratified lakes. *Geophysical Research Letters*, *35*(16), 8–12. https://doi.org/10.1029/2008GL034519

Boehrer, B., Golmen, L., Løvik, J. E., Rahn, K., & Klaveness, D. (2013). Thermobaric stratification in very deep Norwegian freshwater lakes. *Journal of Great Lakes Research*, *39*(4), 690–695. https://doi.org/10.1016/j.jglr.2013.08.003

Boehrer, B., & Schultze, M. (2008). Stratification of lakes. *Reviews of Geophysics*, *46*(2), 1–27. https://doi.org/10.1029/2006RG000210

Bouffard, D., & Wüest, A. (2019). Convection in Lakes. *Annual Review of Fluid Mechanics*, *51*(1), 189–215. https://doi.org/10.1146/annurev-fluid-010518-040506

Brenner, S. (2017). *The free oscillatory response of fjord-type multi-armed lakes*. University of British Columbia.

Cael, B. B., Heathcote, A. J., & Seekell, D. A. (2017). The volume and mean depth of Earth's lakes. *Geophysical Research Letters*, *44*(1), 209–218. https://doi.org/10.1002/2016GL071378

Carmack, E. C., & Weiss, R. F. (1991). Convection in Lake Baikal: An Example of Thermobaric Instability. *Elsevier Oceanography Series*, *57*(C), 215–228.

https://doi.org/10.1016/S0422-9894(08)70069-2

Carmack, E. C., Wiegand, R. C., Daley, R. J., Gray, C. B. J., Jasper, S., Pharo, C. H., … Rao, Y. R. (1991). Formation of the well-mixed homogeneous layer in the bottom water of the Japan Sea. *Limnology and Oceanography*, *59*(2), 249–265. https://doi.org/10.1007/s10584-018-2275-2

Chen, C. A., & Millero, F. J. (1986). Thermodynamic Properties for Natural Waters Covering Only the Limnological Range. *Limnology and Oceanography*, *31*(3), 657–662. https://doi.org/10.4319/lo.1986.31.3.0657

Crawford, G. B., & Collier, R. W. (1997). Observations of a deep-mixing event in Crater Lake, Oregon. *Limnology and Oceanography*, *42*(2), 299–306. https://doi.org/10.4319/lo.1997.42.2.0299

Crawford, G. B., & Collier, R. W. (2007). Long-term observations of deepwater renewal in Crater Lake, Oregon. *Hydrobiologia*, *574*(1), 47–68. https://doi.org/10.1007/s10750-006-0345-3

Eklund. (1965). Stability of Lakes near the Temperature of Maximum Density. *American Association for the Advancement of Science*, *149*(3684), 632–633. Retrieved from https://www.jstor.org/stable/1716666

Farmer, D. M., & Carmack, E. (1981a). Wind mixing and restratification in a lake near the temperature of maximum density. *J. Phys. Oceanogr*. https://doi.org/10.1175/1520-0485(1981)011<1516:wmaria>2.0.co;2

Farmer, D. M., & Carmack, E. C. (1981b). Wind Mixing and Restratification in a Lake near the Temperature of Maximum Density. *J. Phys. Oceanogr.*, *11*.

Gilbert, R., & Desloges, J. R. (2012). Late glacial and Holocene sedimentary environments of Quesnel Lake, British Columbia. *Geomorphology*, *179*, 186–196.

https://doi.org/10.1016/j.geomorph.2012.08.010

Gloor, M., Wüest, A., & Münnich, M. (1994). Benthic boundary mixing and resuspension induced by internal seiches. *Hydrobiologia*, *284*(1), 59–68. https://doi.org/10.1007/BF00005731

Government of Canada. (2019). Williams Lake A. *Historic Weather Data*. https://doi.org/https://climate.weather.gc.ca/historical_data/search_historic_data_e.html?searchType=stnName&timeframe=1&txtStationName=williams+lake&searchMethod=contains&optLimit=yearRange&StartYear=2006&EndYear=2007&Year=2020&Month=7&Day=7&selRowPerPage=25#stnNameTab

Granger, B. (2020). *Suspended sediment in Quesnel Lake following the Mount Polley Mine tailings spill*. University of British Columbia.

Gregory, J. W. (1913). *The Nature and Origin of Fiords*. London: John Murray.

Hamilton, A. K., Laval, B. E., Petticrew, E. L., & Albers, S. J. (2020). Seasonal turbidity linked to physical dynamics in a deep lake following the catastrophic 2014 Mount Polley mine tailings spill. *Water Resources Research*, 0–2. https://doi.org/10.1029/2019WR025790

Hutchinson, G. E., & Loffler, H. (1956). the Thermal Classification of Lakes. *Proceedings of the National Academy of Sciences*, *42*(2), 84–86. https://doi.org/10.1073/pnas.42.2.84

Hutter, K., Wang, Y., & Chubarenko, I. (2011). *Physics of Lakes Volume 1*. London, New York: Springer.

Imberger, J., & Jul, N. (2007). The Diurnal Mixed Layer The diurnal mixed layer1. *Limnology*, *30*(4), 737–770.

Imboden, D. M., & Wuest, A. (1995). Mixing Mechanisms in Lakes. In *Physics and Chemistry of Lakes* (pp. 83–138). https://doi.org/10.1007/978-3-642-85132-2_4

Lamont, C. A. (1991). A Preliminary Review of Enhancement Opportunities for the Thompson River and Quesnel River Drainage Basins. *Unpublished*. Vancouver, BC.

Laval, B. E., Morrison, J., Potts, D. J., Carmack, E. C., Vagle, S., & Vl, B. C. (2008). Wind-driven Summertime Upwelling in a Fjord-type Lake and its Impact on Downstream River Conditions : Quesnel Lake and River, British Columbia, Canada, 189–203.

Laval, B. E., Vagle, S., Potts, D., Morrison, J., Sentlinger, G., James, C., … Carmack, E. C. (2012). The joint effects of riverine, thermal, and wind forcing on a temperate fjord lake: Quesnel Lake, Canada. *Journal of Great Lakes Research*, *38*(3), 540–549. https://doi.org/10.1016/j.jglr.2012.06.007

Lewis Jr., W. M. (1983). A Revised Classification of Lakes Based on Mixing. *Canadian Journal of Fisheries and Aquatic Sciences*. https://doi.org/10.1139/f83-207

Lorke, A., & MacIntyre, S. (2009). Hydrodynamics and Mixing in Lakes , Reservoirs , Wetlands and Rivers. *River Ecosystem Ecology: A Global Perspective. Encyclopedia of Inland Waters*, 505–514.

Lozovatsky, I. D., & Shapovalov, S. M. (2012). Thickness of the mixed bottom layer in the Northern Atlantic. *Oceanology*, *52*(4), 447–452. https://doi.org/10.1134/S0001437012010134

McDougall, T. J. (1987). Thermobaricity, cabbeling, and water-mass conversion. *J. Geophys, Res. 92*, 5448–5464. http://dx.doi.org/10:1016/j.dsr.2003.09.007

Merchant, R. I., & Woolway, C. (2019). Worldwide alteration of lake mixing regimes in response to climate change. *Nature GeoScience*, *12*, 271–276. https://doi.org/10.1038/s41561-019-0322-x

Millero, F. J. (2000). The Equation of State of Lakes. *Aquatic Geochemistry*, *6*, 1–17.

Moore, EJ, Smith, & JW. (1996). Migration in response to climate change, *12*(April), 325–

345. http://apps.isiknowledge.com/full_record.do?product=WOS&search_mode=GeneralSearch&qid=18&SID=3FPNikIfaBIa4L5JfGp&page=1&doc=7

Mount Polley Mining Corporation (MPMC). (2015). Mount Polley Mining Corporation Post Event Environmental Impact Assesment Report, 5405. http://www.imperialmetals.com/assets/docs/mt-polley/2015-06-18-MPMC-KFR.pdf

Nasmith, H. (1962). *Late glacial history and surficail deposits of the Okanagan Valley, British Columbia*. Victoria.

Pawlowicz, R. (2001). Air-Sea Toolbox. Vancouver, BC.

Petticrew, E. L., Albers, S. J., Baldwin, S. A., Carmack, E. C., Déry, S. J., Gantner, N., … Vagle, S. (2015). The impact of a catastrophic mine tailings impoundment spill into one of North America's largest fjord lakes: Quesnel Lake, British Columbia, Canada, 3347–3356. https://doi.org/10.1002/2015GL063345.Received

Piccolroaz, S., & Toffolon, M. (2013). Deep water renewal in lake baikal: A model for long-term analyses. *Journal of Geophysical Research: Oceans*, *118*(12), 6717–6733. https://doi.org/10.1002/2013JC009029

S.W. Hosteler. (n.d.). Hydrological and Thermal Responce of Lakes to Climate: Description and Modeling.

Sebastian, D., Dolighan, R., Andrusak, H., Hume, J., Woodruff, P., & Scholten, G. (2003). *Summary of Quesnel Lake Kokanee and Rainbow Trout Biology With*. Province of British Columbia.

Sharma, A. R., & Déry, S. J. (2016). Elevational dependence of air temperature variability and trends in British Columbia's Cariboo Mountains, 1950-2010. *Atmosphere - Ocean*, *54*(2), 153–170. https://doi.org/10.1080/07055900.2016.1146571

Stevens, C. L., & Lawrence, G. A. (1997). Estimation of wind-forced internal seiche amplitudes in lakes and reservoirs, with data from British Columbia, Canada. *Aquatic Sciences*, *59*(2), 115–134. https://doi.org/10.1007/BF02523176

Syvitsky, J. P. M. ., Burrell, D. C., & Skei, J. M. (1987). *Fjords: Processes and Products*. New York: Springer.

The National Renewable Energy Labority. (n.d.). National Solar Radiation Database. https://www.nrel.gov/

Thompson, H. D. (2019). Wind Climatology of Quesnel Lake, British Columbia, University of Northern British Columbia

UNESCO. (1981). The Practical Salinity Scale 1978 and the International Equation of State of Sea water 1980. *UNESCO Technical Paper Marine Science*, *Vol. 36*. www.jodc.go.jp/../UNESCO_Tech.htm

Vincent, W. F. (2009). Effects of Climate Change on Lakes. *Encyclopedia of Inland Waters*, 55–60. https://doi.org/10.1016/B978-012370626-3.00233-7